

# Site-Selective $C_{sp^3}-C_{sp}/C_{sp^3}-C_{sp^2}$ Cross-Coupling Reactions Using Frustrated Lewis Pairs

Ayan Dasgupta, Katarina Stefkova, Rasool Babaahmadi, Brian F. Yates, Niklaas J. Buurma, Alireza Ariaifard, Emma Richards, and Rebecca L. Melen\*



Cite This: *J. Am. Chem. Soc.* 2021, 143, 4451–4464



Read Online

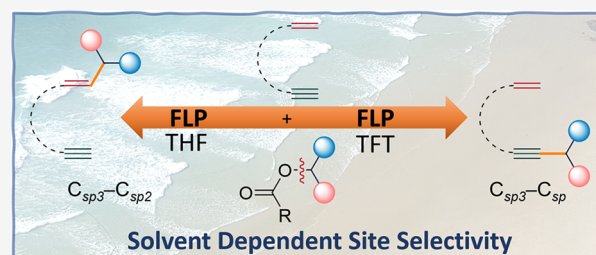
ACCESS |

Metrics & More

Article Recommendations

Supporting Information

**ABSTRACT:** The donor–acceptor ability of frustrated Lewis pairs (FLPs) has led to widespread applications in organic synthesis. Single electron transfer from a donor Lewis base to an acceptor Lewis acid can generate a frustrated radical pair (FRP) depending on the substrate and energy required (thermal or photochemical) to promote an FLP into an FRP system. Herein, we report the  $C_{sp^3}-C_{sp}$  cross-coupling reaction of aryl esters with terminal alkynes using the  $B(C_6F_5)_3/Mes_3P$  FLP. Significantly, when the 1-ethynyl-4-vinylbenzene substrate was employed, the exclusive formation of  $C_{sp^3}-C_{sp}$  cross-coupled products was observed. However, when 1-ethynyl-2-vinylbenzene was employed, solvent-dependent site-selective  $C_{sp^3}-C_{sp}$  or  $C_{sp^3}-C_{sp^2}$  cross-coupling resulted. The nature of these reaction pathways and their selectivity has been investigated by extensive electron paramagnetic resonance (EPR) studies, kinetic studies, and density functional theory (DFT) calculations both to elucidate the mechanism of these coupling reactions and to explain the solvent-dependent site selectivity.

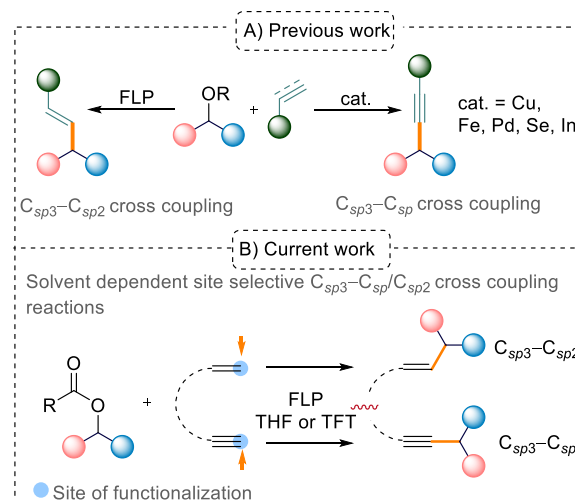


## INTRODUCTION

Frustrated Lewis pairs (FLPs) have garnered much attention over the last two decades, with numerous FLP systems being reported in the literature.<sup>1</sup> The cooperative reactivity of the Lewis acidic and basic components has led to a plethora of different small-molecule activation reactions<sup>2</sup> and catalysis.<sup>3</sup> Current studies have focused on using FLP systems as alternatives or complementary systems to the use of transition-metal catalysts in organic synthesis.<sup>4</sup> Recently, new reactivities of FLPs have been disclosed, indicating that Lewis acids and bases undergo single electron transfer (SET) events<sup>5</sup> depending on the energy required (thermal or photochemical) to promote the FLP into a frustrated radical pair (FRP) system. In these instances, an electron is transferred from the donor Lewis base (LB) to the acceptor Lewis acid (LA) to generate a reactive FRP. Indeed, we and others have postulated that such radical reactivity may be taking place in the reactions of the  $B(C_6F_5)_3/Mes_3P$  FLP with certain substrates.<sup>6</sup> The radical reactivity of FLPs has the potential to open up new opportunities for metal-free synthesis. In a previous study of the  $B(C_6F_5)_3/Mes_3P$  FLP with diaryl esters and alkenes, we observed  $C_{sp^3}-C_{sp^2}$  coupling reactions. We proposed a radical mechanism for the reaction based on the observation of  $[Ar_2CH]^\bullet$  and  $[Mes_3P]^{+\bullet}$  in electron paramagnetic resonance (EPR) studies (Scheme 1A).

In this current study, we were interested in the reactions of FLPs with alkynes in the presence of aryl esters (Scheme 1B). The 1,2-trans-addition of the Lewis acidic and basic

**Scheme 1. (A) Previous Work on Metal-Catalyzed  $C_{sp^3}-C_{sp}$  Cross-Coupling Reactions and FLP-Mediated  $C_{sp^3}-C_{sp^2}$  Cross Coupling and (B) This Work on FLP-Mediated, Solvent-Dependent, Site-Selective  $C_{sp^3}-C_{sp}/C_{sp^3}-C_{sp^2}$  Cross-Coupling Reactions**



Received: February 9, 2021

Published: March 15, 2021

components of FLPs to alkynes is well established<sup>7</sup> and has also been employed in catalytic transformations.<sup>8</sup> Interestingly, when using terminal acetylenes such as phenylacetylene (PhC≡CH) with stronger bases such as *t*Bu<sub>3</sub>P or TMP, deprotonation occurs instead of 1,2-addition to the alkyne generating [LBH][PhC≡CB(C<sub>6</sub>F<sub>5</sub>)<sub>3</sub>] salts.<sup>7c</sup> In transition-metal chemistry, the activation of terminal alkynes for cross-coupling reactions is commonplace in the synthetic chemist's toolbox to construct carbon–carbon bonds.<sup>9</sup> For example, palladium- or copper-catalyzed Sonogashira cross-coupling reactions of terminal alkynes with aryl or alkenyl halides have been used for C<sub>sp</sub><sup>3</sup>–C<sub>sp</sub><sup>2</sup> coupling.<sup>10</sup> In this study, we are interested in the less well reported C<sub>sp</sub><sup>3</sup>–C<sub>sp</sub> coupling reactions. Typically, palladium<sup>11</sup> or earth-abundant metal catalysts such as iron<sup>12</sup> and copper<sup>13</sup> are employed for these reactions, although examples are known with other elements such as indium<sup>14</sup> as well as stoichiometric reactions using Brønsted<sup>15</sup> and Lewis acids.<sup>16</sup>

Herein, we report the high reactivity of frustrated Lewis pairs in selective C<sub>sp</sub><sup>3</sup>–C<sub>sp</sub> coupling reactions between aryl esters and terminal alkynes or 1-ethynyl-4-vinylbenzene. We also report solvent-dependent site selectivity when using 1-ethynyl-2-vinylbenzene as a substrate leading to selective C<sub>sp</sub><sup>3</sup>–C<sub>sp</sub> or C<sub>sp</sub><sup>3</sup>–C<sub>sp</sub><sup>2</sup> cross-coupling depending upon the solvent employed.

## RESULTS AND DISCUSSION

**Reaction Optimization and Development.** Initially, the FLP-mediated C<sub>sp</sub><sup>3</sup>–C<sub>sp</sub> cross-coupling reaction between bis(4-

**Table 1. Optimization of the Reaction Conditions for C<sub>sp</sub><sup>3</sup>–C<sub>sp</sub> Cross-Coupling Reactions<sup>a</sup>**

entry	LA	LB	solvent	temp (°C)	yield (%)
1			toluene	70	0
2		Mes <sub>3</sub> P	toluene	70	0
3	B(C <sub>6</sub> F <sub>5</sub> ) <sub>3</sub>		toluene	70	22
4 <sup>b</sup>	B(C <sub>6</sub> F <sub>5</sub> ) <sub>3</sub>		toluene	70	5
5	B(C <sub>6</sub> F <sub>5</sub> ) <sub>3</sub>	Mes <sub>3</sub> P	toluene	70	54
6	B(C <sub>6</sub> F <sub>5</sub> ) <sub>3</sub>	Mes <sub>3</sub> P	toluene	21	18
7	B(C <sub>6</sub> F <sub>5</sub> ) <sub>3</sub>	Mes <sub>3</sub> P	toluene	110	45
8	B(C <sub>6</sub> F <sub>5</sub> ) <sub>3</sub>	Mes <sub>3</sub> P	THF	70	83
9	B(C <sub>6</sub> F <sub>5</sub> ) <sub>3</sub>	Mes <sub>3</sub> P	TFT	70	71
10	B(C <sub>6</sub> F <sub>5</sub> ) <sub>3</sub>	Mes <sub>3</sub> P	CH <sub>2</sub> Cl <sub>2</sub>	45	38
11	B(C <sub>6</sub> F <sub>5</sub> ) <sub>3</sub>	Mes <sub>3</sub> P	hexane	70	0
12	BF <sub>3</sub> ·OEt	Mes <sub>3</sub> P	toluene	70	0
13	BPh <sub>3</sub>	Mes <sub>3</sub> P	toluene	70	0
14	CF <sub>3</sub> SO <sub>3</sub> H	Mes <sub>3</sub> P	THF	70	0
15	B(C <sub>6</sub> F <sub>5</sub> ) <sub>3</sub>	<i>t</i> Bu <sub>3</sub> P	toluene	70	45
16	B(C <sub>6</sub> F <sub>5</sub> ) <sub>3</sub>	Ph <sub>3</sub> P	THF	70	0
17	B(C <sub>6</sub> F <sub>5</sub> ) <sub>3</sub>	<i>o</i> -tol <sub>3</sub> P	THF	70	0
18	B(C <sub>6</sub> F <sub>5</sub> ) <sub>3</sub>	TMP	THF	70	0
19	B(C <sub>6</sub> F <sub>5</sub> ) <sub>3</sub>	DABCO	THF	70	0
20	B(C <sub>6</sub> F <sub>5</sub> ) <sub>3</sub>	DMA	THF	70	0

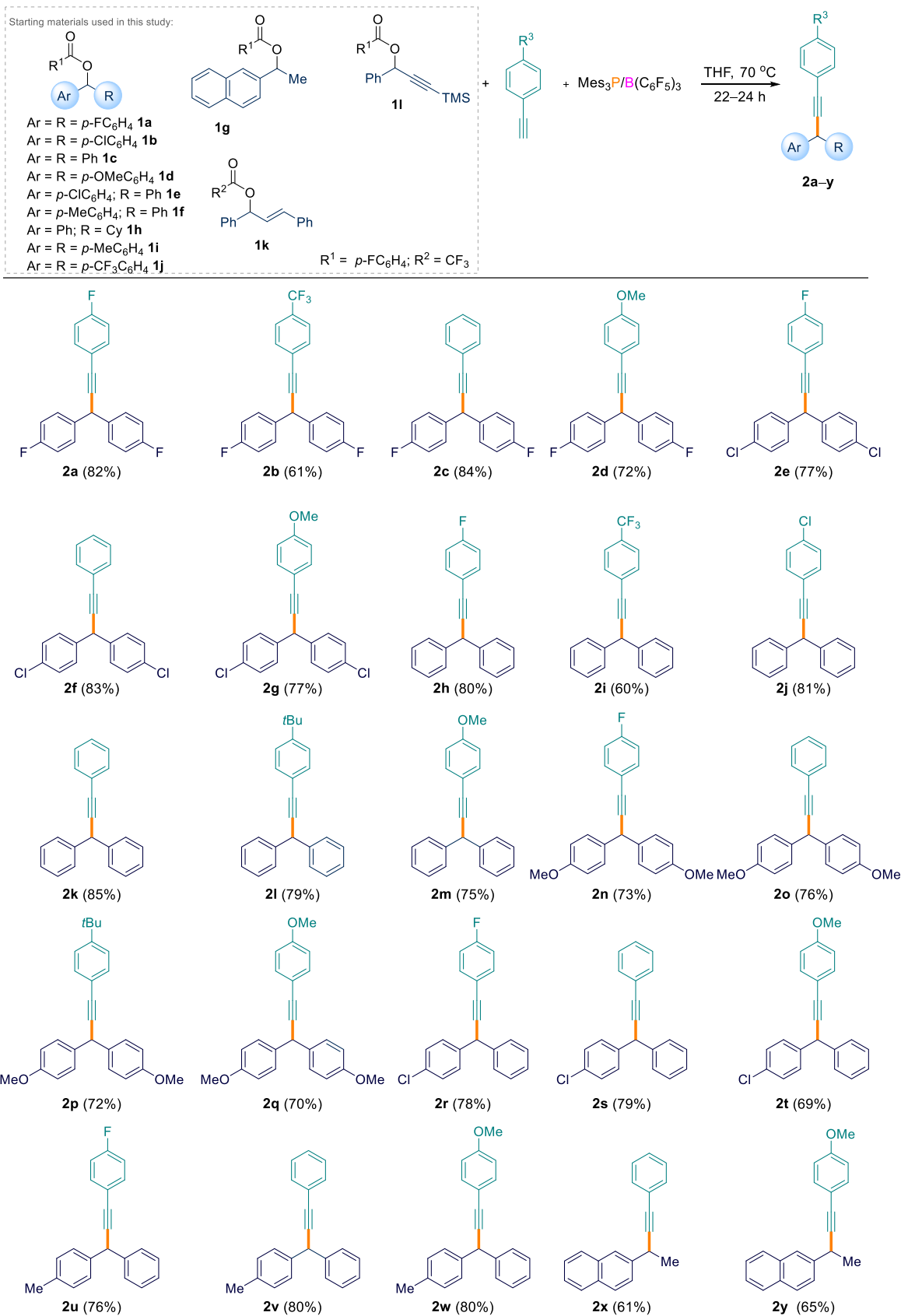
<sup>a</sup>All of the reactions were carried out on a 0.1 mmol scale, and reported yields are isolated. All reactions were carried out for 20–22 h. <sup>b</sup>10 mol % B(C<sub>6</sub>F<sub>5</sub>)<sub>3</sub>.

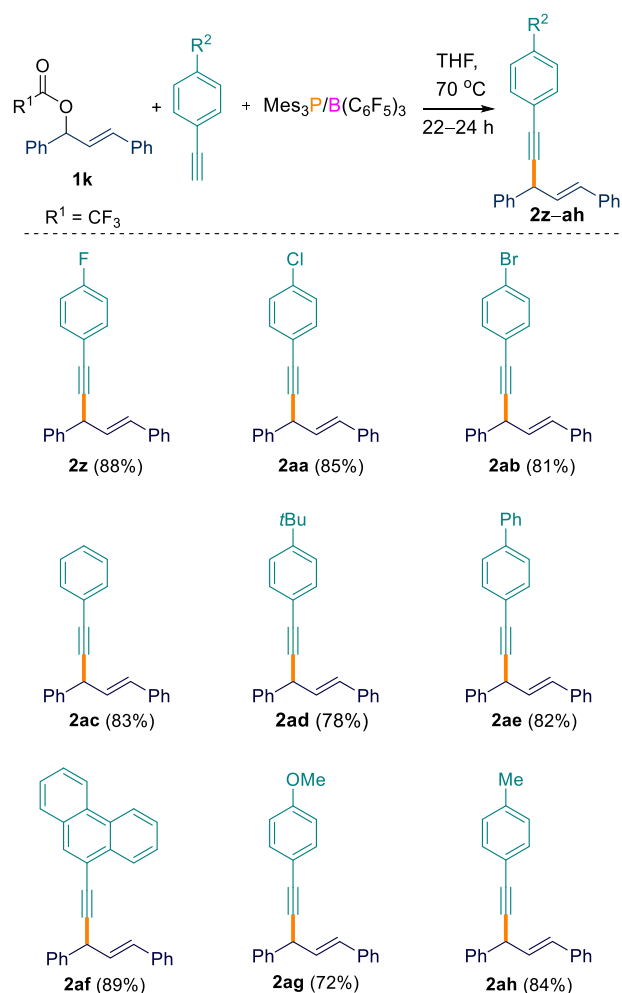
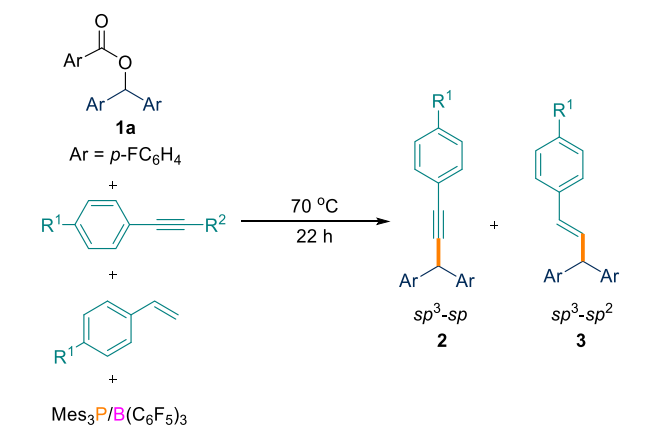
fluorophenyl)methyl-4-fluorobenzoate (**1a**) and phenylacetylene was investigated using a range of reaction conditions (Table 1). As expected, no reaction occurred in the absence of an FLP (Table 1, entry 1). Reaction with only the Lewis base component of the FLP (Mes<sub>3</sub>P) showed no cross-coupled

product, and a stoichiometric or catalytic (10 mol %) amount of the Lewis acid B(C<sub>6</sub>F<sub>5</sub>)<sub>3</sub> led to only 22 and 5% isolated yields of the desired C<sub>sp</sub><sup>3</sup>–C<sub>sp</sub> cross-coupled product, **2a** (Table 1, entries 3 and 4). Stoichiometric amounts of both a Lewis acid and Lewis base were required for the C<sub>sp</sub><sup>3</sup>–C<sub>sp</sub> coupling reaction to attain satisfactory yields of the cross-coupled products. The B(C<sub>6</sub>F<sub>5</sub>)<sub>3</sub>/Mes<sub>3</sub>P FLP in toluene at 70 °C led to the C<sub>sp</sub><sup>3</sup>–C<sub>sp</sub> cross-coupled product, **2a**, being formed in 54% yield (Table 1, entry 5). The optimum temperature was 70 °C with both lower (21 °C) and higher (110 °C) temperatures giving reduced yields (18 and 45% respectively) (Table 1, entries 6 and 7). More polar THF gave the highest yield of 83%, with trifluorotoluene (TFT) giving a 71% yield. CH<sub>2</sub>Cl<sub>2</sub> and hexane, on the other hand, showed poorer or low yields (Table 1, entries 8–11). Interestingly, other Lewis acid boranes (BF<sub>3</sub>·OEt<sub>2</sub> and BPh<sub>3</sub>) as well as Brønsted acids (CF<sub>3</sub>SO<sub>3</sub>H) showed no product formation when combined with Mes<sub>3</sub>P (Table 1, entries 12–14). Other basic phosphines including *t*Bu<sub>3</sub>P, Ph<sub>3</sub>P and *o*-tol<sub>3</sub>P had complicated reaction mixtures with no or moderate yields of **2a** being formed (Table 1, entries 15–17). Nitrogen Lewis bases including TMP (2,2,6,6-tetramethylpiperidine), DABCO (1,4-diazabicyclo(2,2,2)octane), and DMA (4-bromo dimethyl aniline) led to no product formation (Table 1, entries 18–20). The optimum conditions for the reaction were therefore chosen to be the use of the B(C<sub>6</sub>F<sub>5</sub>)<sub>3</sub>/Mes<sub>3</sub>P FLP in THF at 70 °C for 22–24 h.

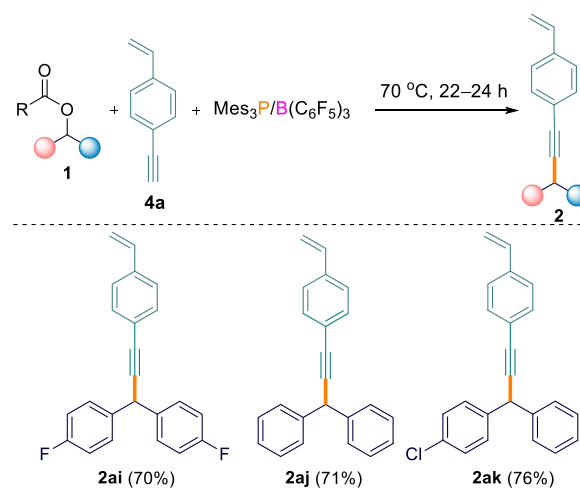
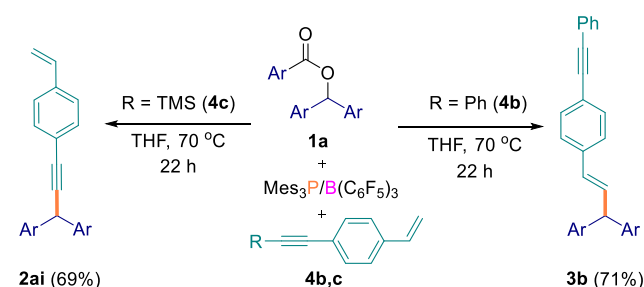
**Reaction Scope.** With the optimized reaction conditions in hand, several aryl esters (**1a–l**) were tested for the FLP-mediated C<sub>sp</sub><sup>3</sup>–C<sub>sp</sub> coupling reaction with various acetylenic compounds (Scheme 2). Diaryl esters bearing electron-withdrawing/ $\pi$ -releasing (*p*-F, **1a**; *p*-Cl, **1b**), neutral (*p*-H, **1c**), and electron-donating (*p*-OMe, **1d**) groups all worked well for the reactions when coupled with aryl-substituted terminal acetylenes with electron-releasing (*p*-OMe, *p*-*t*Bu), neutral (*p*-H), electron-withdrawing/ $\pi$ -releasing (*p*-F, *p*-Cl), and electron-withdrawing (*p*-CF<sub>3</sub>) groups generating products **2a–q** in 60–85% yields. Asymmetrical diaryl esters **1e** and **1f** were also found to undergo the C<sub>sp</sub><sup>3</sup>–C<sub>sp</sub> cross-coupling reaction, with several alkynes generating C–H-functionalized products **2r–w** in excellent isolated yields (69–80%). We could also use alkyl/aryl esters containing just one aryl-stabilizing group. **1g** could be cross-coupled with electron-neutral (phenylacetylene) and electron-releasing (4-ethynylanisole) alkynes to give **2x** and **2y** albeit in slightly lower yields of 61 and 65%, respectively. However, when cyclohexyl-(phenyl)methyl-4-fluorobenzoate (**1h**) was employed, poor conversion was observed. Diaryl esters bearing strongly electron-withdrawing (*p*-CF<sub>3</sub>, **1j**) groups also failed to react at all with terminal alkynes. We attribute this to the electron-deficient nature of the ester which is not Lewis basic enough to form an adduct with the Lewis acidic borane in the initial step of the reaction as observed by *in situ* <sup>11</sup>B and <sup>1</sup>H NMR spectroscopy. The unwillingness of ester **1j** to react with arylacetylenes can also be interpreted from DFT calculations (see later and SI Figure S180).

After achieving good success for the C<sub>sp</sub><sup>3</sup>–C<sub>sp</sub> cross-coupling reaction at the benzylic position, we investigated a wider substrate scope (Scheme 3). To this end, allylic ester (*E*)-1,3-diphenylallyl-2,2,2-trifluoroacetate (**1k**) was used in the C–H functionalization. To our delight, excellent yields of products **2z–ah** (72–89%) were obtained. While benzylic and allylic esters worked well, the same was not true for cross-coupling at

Scheme 2.  $C_{sp^3}-C_{sp}$  Cross-Coupling Reactions between Esters **1** and Acetylenes<sup>a</sup><sup>a</sup>All reactions were performed on a 0.1 mmol scale.

Scheme 3.  $C_{sp^3}-C_{sp}$  Cross-Coupling Reactions between Ester **1k** and Acetylenes<sup>a</sup><sup>a</sup>All reactions were performed on a 0.1 mmol scale.Table 2. Selectivity Reactions between Esters **1a** and Acetylenes/Styrene<sup>a</sup>

entry	$R^1$	$R^2$	solvent	yield $C_{sp^3}-C_{sp}$ (%)	yield $C_{sp^3}-C_{sp^2}$ (%)
1	F	H	THF	78 ( <b>2a</b> )	n.d.
2	F	H	TFT	72 ( <b>2a</b> )	n.d.
3	H	Ph	THF	n.d.	63 ( <b>3a</b> )
4	H	TMS	THF	58 ( <b>2c</b> )	18 ( <b>3a</b> )

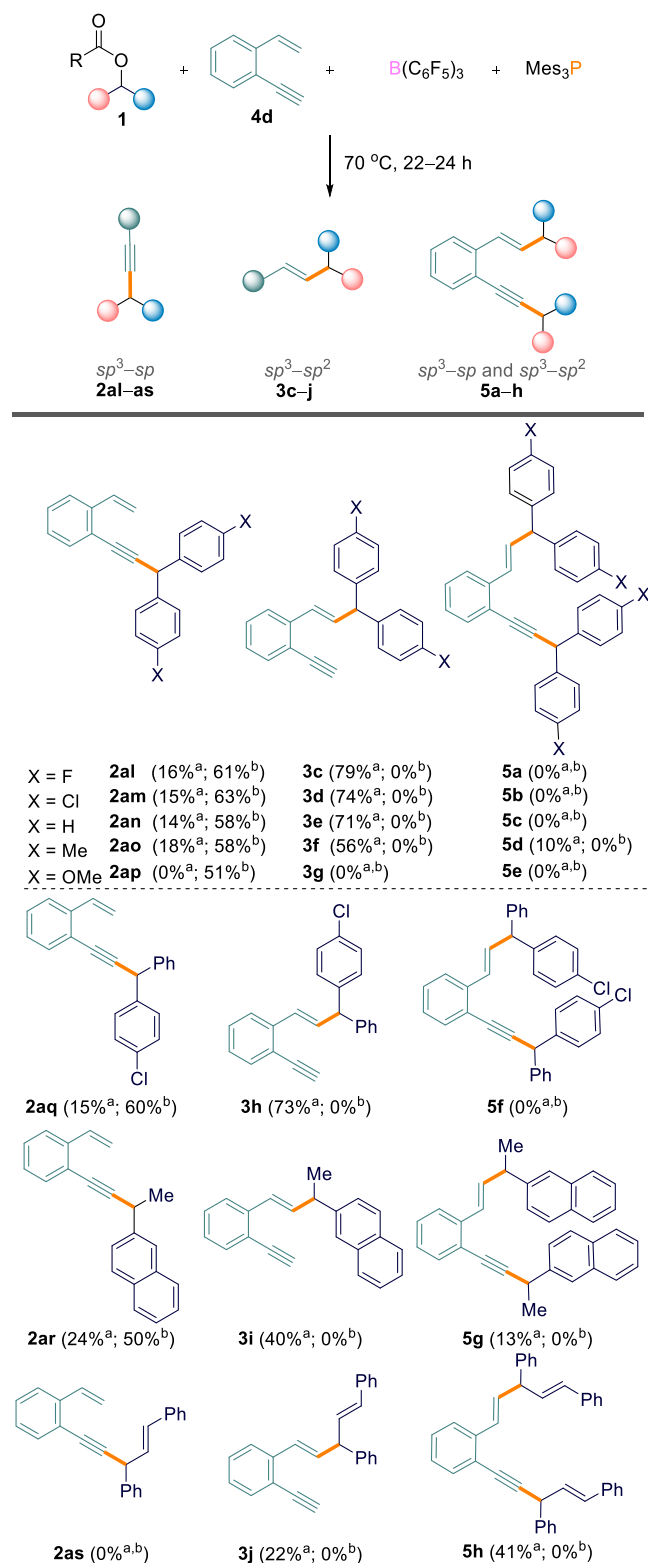
<sup>a</sup>0.1 mmol scale, reported yields are isolated; n.d. = not detected.Scheme 4. Cross-Coupling Reactions between Esters **1a,c,e** and 1-Ethynyl-4-vinylbenzene **4a**<sup>a</sup><sup>a</sup>0.1 mmol scale; reported yields are isolated.Scheme 5. Cross-Coupling Reactions between Ester **1a** and Substrates **4** bearing Internal Alkynes<sup>a</sup><sup>a</sup>All reactions were performed on a 0.1 mmol scale.Table 3. Solvent-Dependent Site-Selective Studies<sup>a</sup>

entry	ester	ratio of 2:3:5 in THF	entry	ester	ratio of 2:3:5 in TFT
1	<b>1a</b>	0.2:1:0	9	<b>1a</b>	1:0:0
2	<b>1b</b>	0.2:1:0	10	<b>1b</b>	1:0:0
3	<b>1c</b>	0.2:1:0	11	<b>1c</b>	1:0:0
4	<b>1i</b>	0.4:1:0.1	12	<b>1i</b>	1:0:0
5	<b>1d</b>	0:0:0	13	<b>1d</b>	1:0:0
6	<b>1e</b>	0.2:1:0	14	<b>1e</b>	1:0:0
7	<b>1g</b>	0.5:1:0.1	15	<b>1g</b>	1:0:0
8	<b>1j</b>	0:1:1.5	16	<b>1j</b>	0:0:0

<sup>a</sup>Ratios were determined from the crude <sup>1</sup>H NMR spectra.

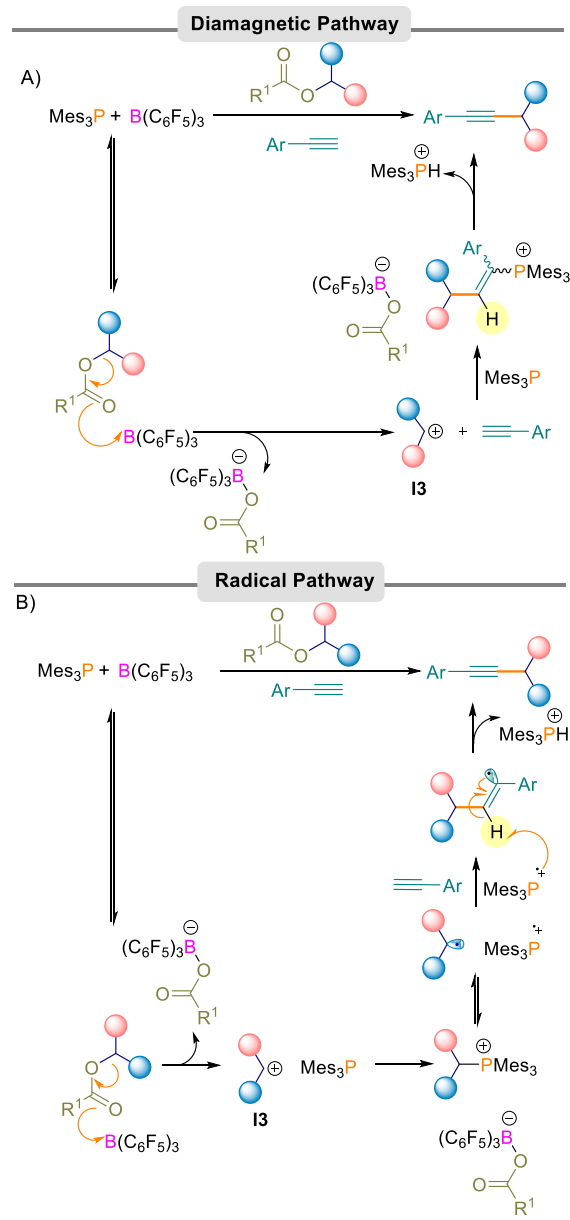
the propargylic position. When the aryl/alkynyl ester 1-phenyl-3-(trimethylsilyl)prop-2-yn-1-yl 4-fluorobenzoate (**11**) was employed with terminal acetylenes, an inseparable complicated reaction mixture resulted.

In our previous studies,<sup>6</sup> we have shown that reactions of esters **1** with styrenes in the presence of the same FLP leads to  $C_{sp^3}-C_{sp^2}$  coupled products. We therefore undertook an experiment to investigate the regioselectivity of the reaction by reacting the ester starting material with a 1:1 mixture of an acetylene and a styrene. For this reaction, three outcomes are theoretically possible: (i) formation of the  $C_{sp^3}-C_{sp}$  coupled product, (ii) formation of the  $C_{sp^3}-C_{sp^2}$  coupled product, or (iii) formation of a mixture of  $C_{sp^3}-C_{sp}$  and  $C_{sp^3}-C_{sp^2}$  coupled products. Using the optimized reaction conditions, an

Scheme 6. Products of Solvent-Dependent Site-Selective Cross-Coupling Reactions<sup>a</sup>

<sup>a</sup>Reactions were carried out on a 0.1 mmol scale, and yields were isolated. <sup>a</sup>Yield in THF. <sup>b</sup>Yield in TFT.

equimolar mixture of aryl ester **1a**, 4-fluorophenylacetylene, and 4-fluorostyrene were reacted together with  $B(C_6F_5)_3/Mes_3P$  (Table 2).

Scheme 7. Possible Reaction Mechanisms<sup>a</sup>

<sup>a</sup>(A) Diamagnetic pathway. (B) Radical pathway.

The crude <sup>1</sup>H NMR spectrum clearly showed a sharp singlet at  $\delta = 5.09$  ppm which confirmed the formation of the  $C_{sp^3}-C_{sp}$  cross-coupled product, **2a**, isolated as the major product in 78% yield (Table 2, entry 1). We were not able to detect any characteristic peaks (i.e., a doublet at  $\delta = 4.98$  ppm in the <sup>1</sup>H NMR spectrum)<sup>6</sup> for the  $C_{sp^3}-C_{sp^2}$  coupled compound. To investigate the effect of solvent on the reaction, we also conducted the reaction in TFT, where again **2a** was isolated as the major product albeit with a slightly reduced yield of 72% (Table 2, entry 2). The observation of exclusive  $C_{sp^3}-C_{sp}$  coupling is presumably a consequence of the higher reactivity of the alkyne functionality over the alkene. A similar competition experiment, using a 1:1 mixture of styrene and the internal alkyne diphenylacetylene, gave only  $C_{sp^3}-C_{sp^2}$  coupling producing **3a** in 63% yield (Table 2, entry 3). Interestingly, TMS-protected alkynes behaved in the same manner as terminal alkynes, predominantly giving the  $C_{sp^3}-C_{sp}$

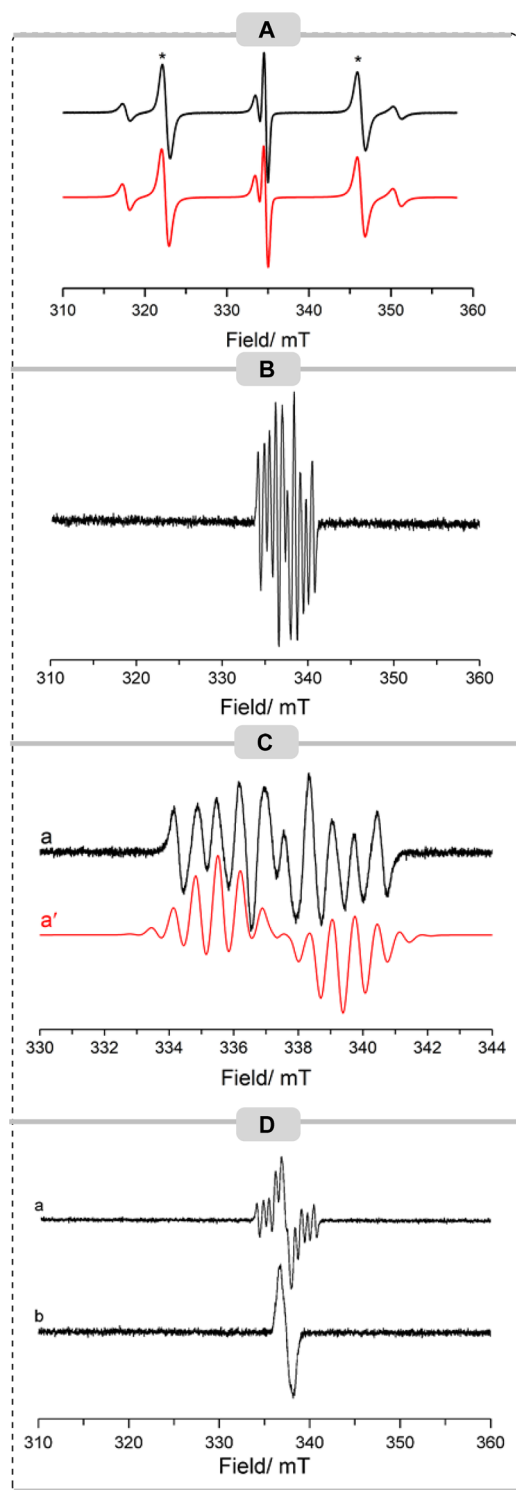
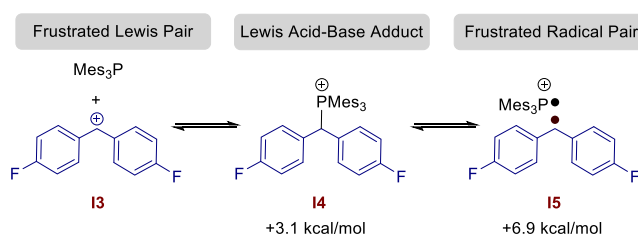


**Figure 1.** CW X-band EPR spectra ( $T = 298$  K) of (A) FLP + ester **1d**, (B) FLP + phenylacetylene, (C) FLP + phenylacetylene (black, experimental; red, simulated), and (D) FLP + phenylacetylene + ester recorded at (a)  $t = 0$  min and (b) after storage at 77 K for 30 min. TFT was used as the solvent for all EPR measurements.

coupled product with the loss of the TMS group. Using a 1:1 mixture of styrene and trimethyl(phenylethynyl)silane afforded the  $C_{sp^3}-C_{sp}$  coupled product (**2c**, 58% isolated) as the major product with small amounts of the  $C_{sp^3}-C_{sp^2}$  cross-coupled product (**3a**, 18% isolated) formed (Table 2, entry 4). This was also observed by *in situ*  $^1H$  NMR spectroscopy of the

### Scheme 8. Mes<sub>3</sub>P/Diaryl Methylene Cation Equilibria in Solution



crude reaction mixture, which displayed a 1:0.4 ratio of  $C_{sp^3}-C_{sp}$  to  $C_{sp^3}-C_{sp^2}$  cross-coupled products.

To demonstrate the scope for this selectivity, we synthesized a substrate containing both alkene and alkyne functionalities, namely, 1-ethynyl-4-vinylbenzene (**4a**).<sup>17</sup> **4a** was subsequently reacted with different aryl esters (**1a,c,e**) in the presence of the  $B(C_6F_5)_3/Mes_3P$  FLP. In agreement with the observation above, we observed only the formation of the  $C_{sp^3}-C_{sp}$  compounds as the major product (**2ai-ak**; 70–76%) using the optimized reaction conditions (Scheme 4). In all cases, the  $C_{sp^3}-C_{sp^2}$  coupled product was either not detected or was observed in <5% yield in both THF and TFT solvents.

As for the intermolecular competition reactions, we also synthesized internal alkynes in which the acetylenic proton in **4a** was replaced by a phenyl or TMS group to explore how this affected the regioselectivity of the reaction (Scheme 5). Using the optimized reaction conditions, the reaction of aryl ester **1a** with 1-(phenylethynyl)-4-vinylbenzene (**4b**) exclusively gave the  $C_{sp^3}-C_{sp^2}$  cross-coupled product in 71% isolated yield from the reaction with the alkene, whereas when **1a** was reacted with trimethyl{(4-vinylphenyl)ethynyl}silane (**4c**), reaction at the alkyne and removal of the TMS group *in situ* afforded the  $C_{sp^3}-C_{sp}$  cross-coupled product (**2ai**) in 69% yield, with no significant reaction at the alkene site observed.

With these results in hand, we further explored the substrate scope using the 1-ethynyl-2-vinylbenzene (**4d**).<sup>18</sup> **4d** was reacted with ester **1a** and the  $B(C_6F_5)_3/Mes_3P$  FLP under the optimized reaction conditions (THF, 70 °C, 24 h). Contrary to the reactions above, the reactions were found to be highly site-selective for the  $C_{sp^3}-C_{sp^2}$  coupled product, **3**, from reaction at the alkene functional group. Examining the crude  $^1H$  NMR spectrum revealed a 0.2:1:0 ratio of the products ( $C_{sp^3}-C_{sp}$  coupled, **2**)/( $C_{sp^3}-C_{sp^2}$  coupled, **3**)/( $C_{sp^3}-C_{sp}$  and  $C_{sp^3}-C_{sp^2}$  coupled, **5**) (Table 3, entry 1) with isolated yields of 79% for the  $C_{sp^3}-C_{sp^2}$  coupled product, **3c**, and 16% for the  $C_{sp^3}-C_{sp}$  coupled product, **2al** (Scheme 6). Interestingly, when changing the solvent to TFT, the selectivity was completely reversed, exclusively giving  $C_{sp^3}-C_{sp}$  product **2al** from reaction at the alkyne site.

This was observed by crude  $^1H$  NMR, indicating a 1:0:0 ratio of 2/3/5 (Table 3, entry 9) in which **2al** could be isolated in 61% yield (Scheme 6). Remarkably, by simply changing the solvent we can switch the site selectivity of the reaction.

We next investigated this solvent-dependent site selectivity for a range of other esters and found the same general trend. In the following discussion, all reaction product ratios were determined via crude  $^1H$  NMR studies and are listed in Table 3, with the corresponding isolated yields for the products shown in Scheme 6. Initially, we explored the reactions in THF solvent. When electron-withdrawing aryl esters **1b** (*p*-Cl) or electron-neutral symmetrical diaryl esters **1c** (*p*-H) and **1i** (*p*-Me) were

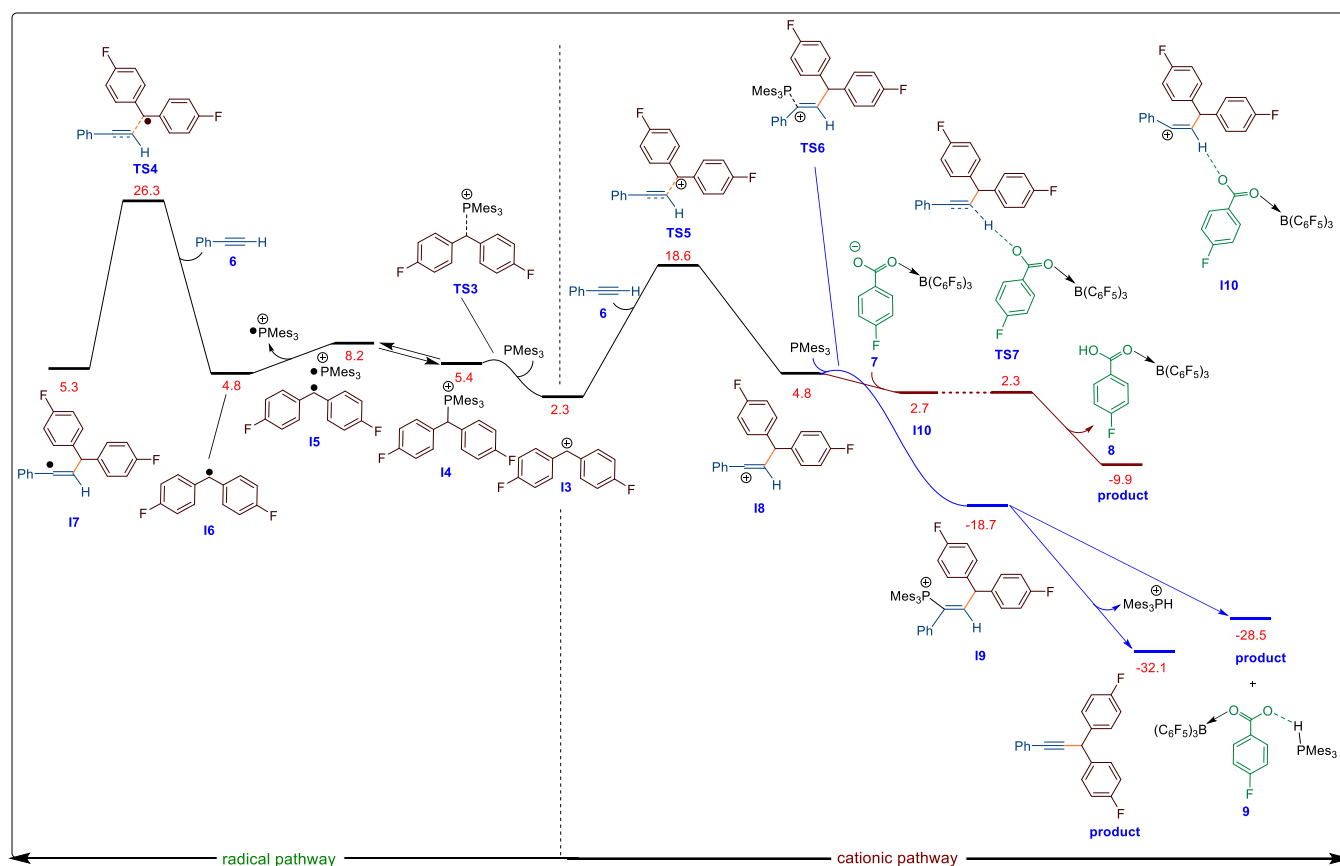


**Figure 2.** DFT-computed reaction pathways for the reaction of **13** with phenylacetylene calculated by SMD/B3LYP-D3/def2-TZVP//SMD/B3LYP-D3/6-31G(d) in THF. The relative free energies are given in kcal/mol. For this energy profile, structure **1a** is set as the reference point as indicated in Figure S178.

**Table 4.** DFT-Computed  $TS_{4, \text{radical pathway}}$  and  $TSS_{\text{cationic pathway}}$  for the Reaction of **1a**, **d**, or **j** with Various Arylacetylenes ( $p\text{-XC}_6\text{H}_4\text{C}\equiv\text{CH}$ ) Calculated by SMD/B3LYP-D3/def2-TZVP//SMD/B3LYP-D3/6-31G(d) in THF<sup>a</sup>

entry	ester (Ar)	X	$TS_{4, \text{radical pathway}}$	$TSS_{\text{cationic pathway}}$
1	<b>1a</b> ( $p\text{-FC}_6\text{H}_4$ )	NO <sub>2</sub>	23.9	23.2
2	<b>1a</b> ( $p\text{-FC}_6\text{H}_4$ )	CF <sub>3</sub>	26.2	20.1
3	<b>1a</b> ( $p\text{-FC}_6\text{H}_4$ )	H	26.3	18.6
4	<b>1a</b> ( $p\text{-FC}_6\text{H}_4$ )	OMe	26.0	13.9
5	<b>1a</b> ( $p\text{-FC}_6\text{H}_4$ )	NMe <sub>2</sub>	27.0	8.2
6	<b>1d</b> ( $p\text{-OMeC}_6\text{H}_4$ )	CF <sub>3</sub>	23.7	13.0
7	<b>1d</b> ( $p\text{-OMeC}_6\text{H}_4$ )	OMe	27.8	8.1
8	<b>1j</b> ( $p\text{-CF}_3\text{C}_6\text{H}_4$ )	CF <sub>3</sub>	24.1	25.5
9	<b>1j</b> ( $p\text{-CF}_3\text{C}_6\text{H}_4$ )	OMe	22.2	17.5

<sup>a</sup>The relative free energies are given in kcal/mol.

used, there was a clear preference for reaction at the alkene site leading to  $C_{sp^3}\text{-}C_{sp^2}$  coupled products **3d**, **3e**, and **3f** in ratios of 0.2:1:0, 0.2:1:0, and 0.4:1:0.1 for **2/3/5**, respectively (Table 3, entries 2–4). In all cases, the major and minor regioisomers could be separated. The  $C_{sp^3}\text{-}C_{sp^2}$  cross-coupled products were isolated in 74% (**3d**), 71% (**3e**), and 56% (**3f**) yields, and the  $C_{sp^3}\text{-}C_{sp}$  cross-coupled products were isolated in 15% (**2am**), 14% (**2an**), and 18% (**2ao**) yields. In the case of **1i** as the starting material, double cross-coupled product **5d** was observed in small amounts and could be separated and isolated in 10% yield (Scheme 6). Electron-rich  $p\text{-OMe}$  ester

**1d**, on the other hand, showed no reactivity at all in THF (Table 3, entry 5). Asymmetrical diaryl ester **1e** gave a ratio of 0.2:1:0 for **2/3/5** (Table 3, entry 6), with **2aq** and **3h** being isolated in 15 and 73% yields, respectively. Alkyl/aryl ester **1g** also gave the  $C_{sp^3}\text{-}C_{sp^2}$  cross-coupled product as the major isomer, albeit less selectively, showing a 0.5:1:0.1 ratio of the three products **2ar/3i/5g** in isolated yields of 24% (**2ar**), 40% (**3i**), and 13% (**5g**) (Table 3, entry 7 and Scheme 6). 1,3-Diphenylallyl-2,2,2-trifluoroacetate (**1k**), on the other hand, showed a preference for the double cross-coupled product, giving a 0:1:1.5 ratio of **2/3/5** with isolated yields of 22% (**3j**) and 41% (**5h**) (Table 3, entry 8 and Scheme 6).

Subsequently, we repeated the above series of reactions in TFT, and remarkably, the regioselectivity was altered and the selectivity was improved. No  $C_{sp^3}\text{-}C_{sp^2}$  coupled product (**3**) or double  $C_{sp^3}\text{-}C_{sp}/C_{sp^3}\text{-}C_{sp^2}$  coupled product (**5**) was observed with any combination of substrates. Rather, a ratio of 1:0:0 of products **2/3/5** was observed in all cases for esters **1a–e**, **1g**, and **1i** (Table 3, entries 9–15). This included  $p\text{-OMe}$  ester **1d** which did not show any product formation in THF.  $C_{sp^3}\text{-}C_{sp}$  cross-coupled products **2al–ar** could be isolated in 50–63% yields (Scheme 6). The only exception was 1,3-diphenylallyl 2,2,2-trifluoroacetate (**1k**), which gave a complex mixture of inseparable products when reacted with 1-ethynyl-2-vinylbenzene (**4d**) in TFT, none of which could be identified as **2**, **3**, or **5** (Table 2, entry 16).

**Proposed Reaction Mechanism.** The  $C_{sp^3}\text{-}C_{sp}$  cross-coupling reaction could be explained by either a single- or a two-electron pathway.

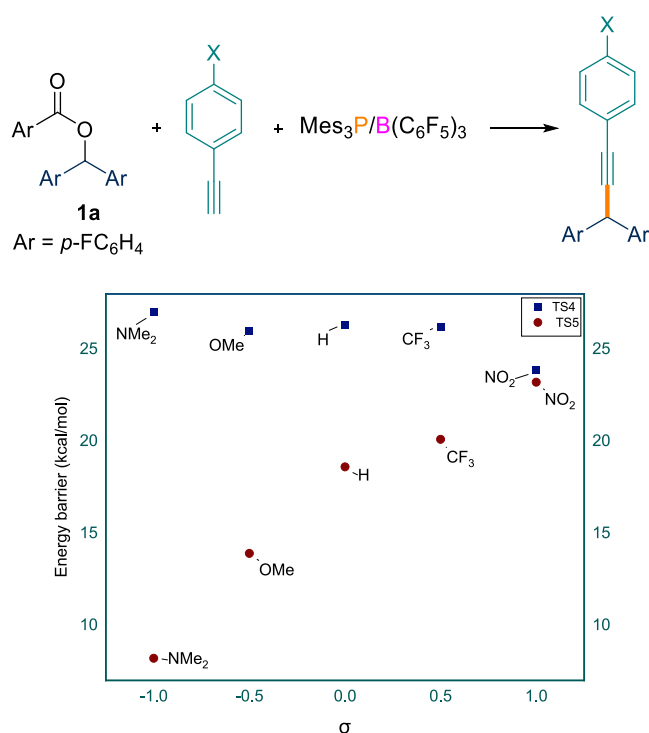


**Figure 3.** DFT (SMD/B3LYP-D3/def2-TZVP//SMD/B3LYP-D3/6-31G(d) in THF)-computed energy barrier (TS4 and TSS, Table 3; entry 1–5) plotted as a function of the Hammett-substituent constant in a Hammett-style plot. The relative free energies are given in kcal/mol.

**Table 5. Competitive Reaction among 1a, Different Acetylenes, and the FLP**

entry	X	X'	product ratio	$k_x/k_{x'}$
1	OMe	H	(2d:2c) 14.3:1	21.9
2	CF <sub>3</sub>	H	(2b:2c) 0.12:1	0.082
3	OMe	CF <sub>3</sub>	(2d:2b) 1: < 0.05	

First, a diamagnetic pathway could operate (Scheme 7A) in which the Lewis acid component of the FLP activates the ester carbonyl atom, leading to the formation of diaryl methylene cation **I3** and the borate anion  $[\text{R}^1\text{CO}_2\text{B}(\text{C}_6\text{F}_5)_3]^-$ . This was observed in our previous studies when  $\text{B}(\text{C}_6\text{F}_5)_3$  was added to the diaryl ester in the presence of a nucleophile to trap the resultant carbocation.<sup>19</sup> The diaryl methylene cation and the Lewis basic component of the FLP can then undergo a 1,2-FLP addition to the alkyne similar to other FLP 1,2-additions.<sup>20</sup> Finally, the elimination of  $[\text{Mes}_3\text{P}]\text{H}^+$  leads to the C–C bonded product and salt  $[\text{R}^1\text{CO}_2\text{B}(\text{C}_6\text{F}_5)_3][\text{HPMes}_3]$  ( $\text{R}^1 = p\text{-FC}_6\text{H}_4$  or  $\text{CF}_3$ ). This can be observed in the reaction by multinuclear NMR spectroscopy showing a clear  $^1\text{J}_{\text{PH}}$  coupling of 479.5 Hz.

Alternatively, a radical pathway could operate (Scheme 7B), which may explain the necessity for using  $\text{Mes}_3\text{P}$  as a Lewis base rather than other phosphine or nitrogen bases. Previous

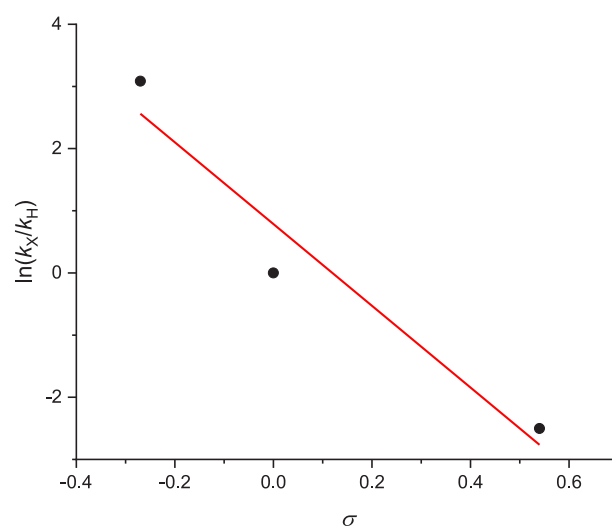


**Figure 4.** Hammett plot for the reaction of **I3** with arylacetylenes.

studies have postulated that the  $\text{B}(\text{C}_6\text{F}_5)_3/\text{Mes}_3\text{P}$  FLP can undergo a single electron transfer (SET) process generating radical ion pair  $[\text{B}(\text{C}_6\text{F}_5)_3]^{*-}/[\text{Mes}_3\text{P}]^{*+}$ .<sup>21</sup> Slootweg et al. later postulated that this process is promoted upon irradiation with visible light (390–500 nm).<sup>5b</sup> In this pathway (Scheme 7B), we propose that the first step of the reaction is identical to the diamagnetic pathway whereby  $\text{B}(\text{C}_6\text{F}_5)_3$  activates the diaryl ester to generate diaryl methylene cation **I3** and borate anion  $[\text{R}^1\text{CO}_2\text{B}(\text{C}_6\text{F}_5)_3]^-$ . The Lewis base then reacts with cation **I3**, forming a Lewis acid–base adduct. We propose that this adduct is in equilibrium with diaryl methylene radical  $[\text{Ar}_2\text{CH}]^*$  and phosphonium radical cation  $[\text{Mes}_3\text{P}]^{*+}$ , which are formed from the homolytic cleavage of the C–P bond. From here, diaryl methylene radical  $[\text{Ar}_2\text{CH}]^*$  adds to arylacetylene, leading to a vinylic radical species which, upon abstraction of a hydrogen atom by  $[\text{Mes}_3\text{P}]^{*+}$ , generates the desired C–C bonded product.

To understand which pathway is operating, we undertook extensive electron paramagnetic resonance (EPR), kinetic, and density functional theory (DFT) studies to understand the reaction mechanism for the  $\text{C}_{\text{sp}^3}\text{--}\text{C}_{\text{sp}}$  coupling reaction.

**EPR Studies.** The knowledge that the  $\text{B}(\text{C}_6\text{F}_5)_3/\text{Mes}_3\text{P}$  FLP can generate radical species prompted us to undertake an EPR study to determine if radical species could be observed in these reactions. As reported previously, no EPR signal could be detected from the  $\text{B}(\text{C}_6\text{F}_5)_3/\text{Mes}_3\text{P}$  FLP in the absence of any substrates.<sup>21</sup> Upon addition of an equimolar ratio of ester **1d** to the FLP in a TFT solution, several EPR signals arising from multiple paramagnetic species were detected at room temperature (Figure 1A). Upon comparison with previous reports, the two intense resonance lines in a 1:1 ratio (marked with asterisks) centered on  $g_{\text{iso}} = 2.012$  ( $B \approx 335$  mT) and separated by a phosphorus hyperfine splitting of  $a_{\text{iso}}(^{31}\text{P}) = 670$  MHz (23.8 mT) are attributed to the formation of the  $[\text{Mes}_3\text{P}]^{*+}$  cation.<sup>22</sup> A second paramagnetic species was also detected in this sample, which is characterized by a 1:2:1 triplet centered on  $g_{\text{iso}} = 2.010$  and separated by a hyperfine splitting of 470 MHz (16.7 mT). This EPR profile must originate from two identical  $I = 1/2$  nuclei, in this case associated with two equivalent  $^{31}\text{P}$  nuclei. The signal is therefore tentatively assigned to the formation of a  $[(\text{P}(\text{Mes})_{n=2,3})_2]^{*+}$  dimer formed from the association of excess  $\text{Mes}_3\text{P}$  with radical cation  $[\text{Mes}_3\text{P}]^{*+}$  as observed previously.<sup>23</sup> This assignment is

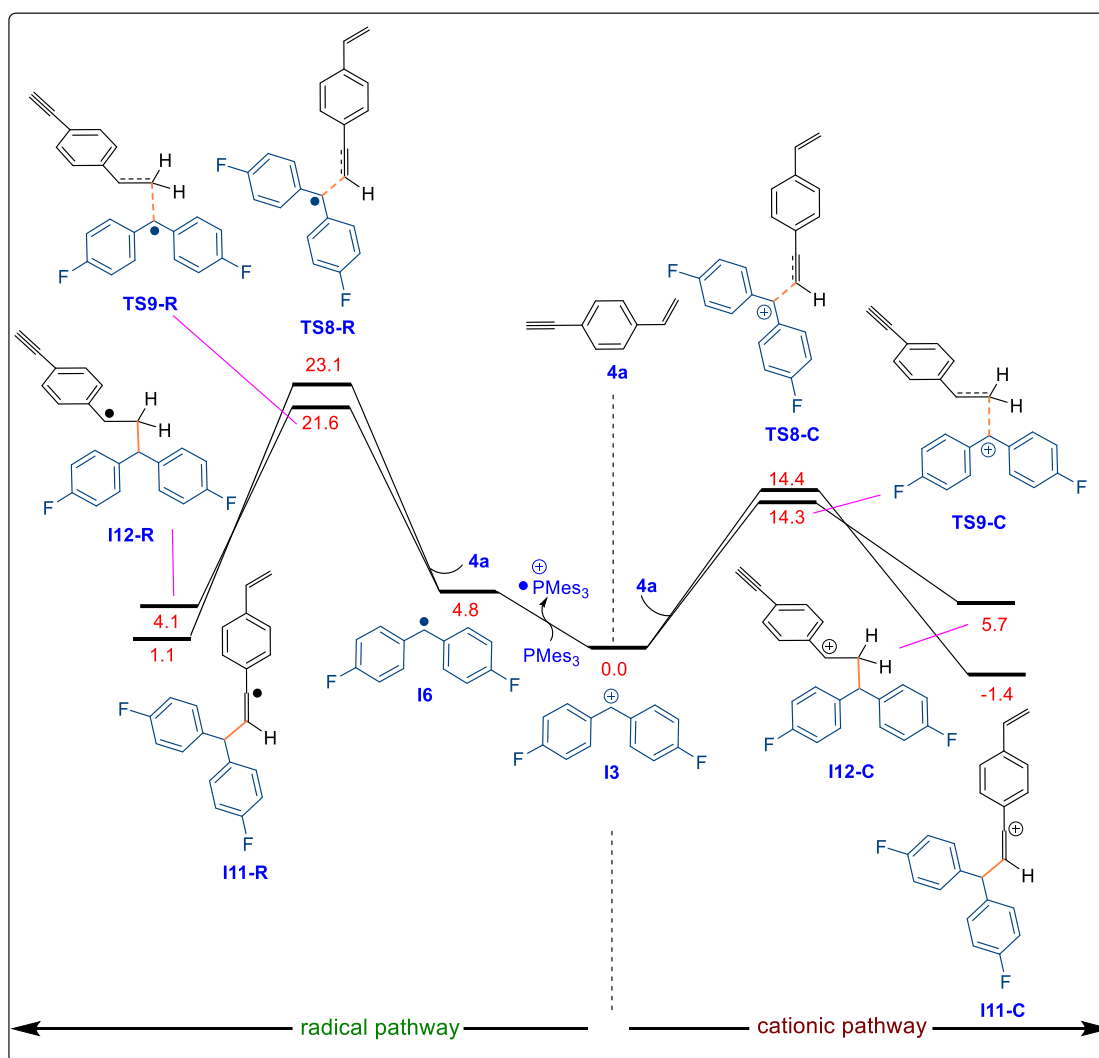


**Figure 5.** DFT-computed reaction pathways for the reaction of **I3** with 1-ethynyl-4-vinylbenzene (**4a**) and  $\text{Mes}_3\text{P}$  calculated using the SMD/B3LYP-D3/def2-TZVP//SMD/B3LYP-D3/6-31G(d) level of theory in THF.

supported by our observation that the relative ratios of the EPR signals of  $[\text{Mes}_3\text{P}]^{\bullet+}/[(\text{P}(\text{Mes})_{n=2,3})_2]^{\bullet+}$  are inter-related (i.e., when a large signal intensity of the monomer is observed, only a trace of the corresponding dimer is detected). The varying ratio of these EPR signals under different reaction conditions demonstrates the conversion between monomer and dimer via the reaction of the monomer with a second molecule of phosphine to yield the dimer radical cation, as previously observed for a series of phosphines,<sup>24</sup> and possibly also the varying stabilities of the two radical species. The EPR spectrum of  $[(\text{P}(\text{Mes}_2)_2)]^{\bullet+}$  has previously been reported,<sup>25</sup> characterized by  $g_{\text{iso}} = 2.006$  and  $a_{\text{iso}}(^{31}\text{P}) = 474$  MHz (17 mT), and it is noted that literature examples of phosphine dimer cation radicals of divalent  $(\text{R}_2\text{P})_2^{\bullet+}$  and trivalent  $(\text{R}_3\text{P})_2^{\bullet+}$  systems yield very similar EPR spectra,<sup>26</sup> dominated by the 1:2:1 phosphorus hyperfine splitting.

The corresponding anisotropic EPR spectra of the  $[\text{Mes}_3\text{P}]^{\bullet+}$  monomer and  $[(\text{P}(\text{Mes})_{n=2,3})_2]^{\bullet+}$  dimer species in frozen solutions are shown in the SI (Figure S176), from which the principal values of the  $g$  and  $A$  tensors were determined. The spin Hamiltonian parameters for all of the paramagnetic species detected in this work are listed in the SI (Table S1). Importantly, contrary to our previous reports,<sup>6</sup> no evidence for

the formation of the carbon-based bismethoxy-diphenylmethylene radical formed upon C–O bond cleavage was observed in this case, perhaps due to the instability of the radical species.

We then probed the room-temperature EPR spectrum of the FLP in the presence of phenylacetylene (Figure 1B,C). Under these experimental conditions, we postulated that another possible mechanism could be the abstraction of the terminal hydrogen atom of the acetylene by the  $[\text{Mes}_3\text{P}]^{\bullet+}$  radical cation to form the diamagnetic  $[\text{Mes}_3\text{PH}]^+$  cation and the corresponding phenylacetylene radical. As can be seen from the wide field scanning range in Figure 1B, no evidence of monomer  $[\text{Mes}_3\text{P}]^{\bullet+}$  or dimer  $[(\text{P}(\text{Mes})_{n=2,3})_2]^{\bullet+}$  was observed in this solution, suggesting the formation of the diamagnetic  $[\text{Mes}_3\text{PH}]^+$  cation. However, no EPR evidence for the generation of the phenylacetylene radical was obtained. It is noted in previous literature studies that the terminal phenylacetylene radical is inherently unstable and is typically observed only via EPR spectroscopy under controlled conditions, such as neat liquids sealed under vacuum, or via matrix isolation methods.<sup>27</sup> Notably, the remaining boron component of the FLP is not involved in the above hydrogen atom abstraction from the alkyne and may be expected to

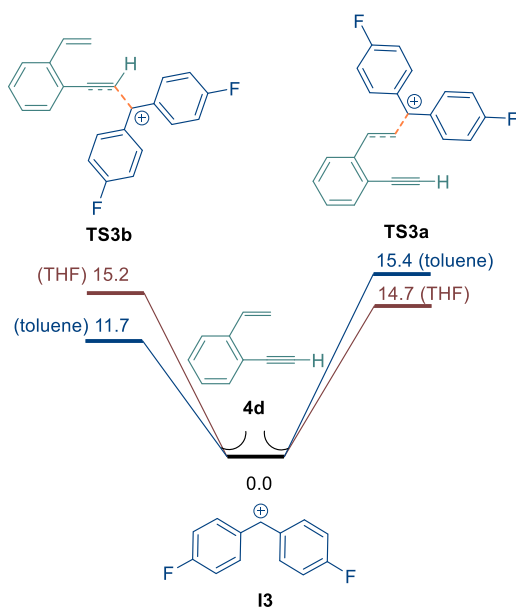


**Figure 6.** DFT calculations of the site selectivity of **I3** with 1-ethynyl-2-vinylbenzene **4d**, calculated at the SMD/B3LYP-D3/def2-TZVP//SMD/B3LYP-D3/6-31G(d) level in THF and toluene.

remain in solution. The intense multiplet signal observed, reproduced in Figure 1C across a narrow field range, is therefore assigned to the boron radical anion,  $[B(C_6F_5)_3]^{•-}$ . A satisfactory simulation of the experimental data was achieved using  $g_{iso} = 2.0114$  and incorporating a single boron nucleus,  $a_{iso}^{(10,11B)} = 27$  MHz, two sets of six equivalent fluorine nuclei from the ortho and meta positions, with  $a_{iso}^{(19F)_{ortho}} = 18.28$  MHz and  $a_{iso}^{(19F)_{meta}} = 3$  MHz, and three para fluorine nuclei with  $a_{iso}^{(19F)_{para}} = 20.2$  MHz, which agrees well with previous literature reports of this species.<sup>28</sup> The corresponding anisotropic spectrum for this sample was unfortunately not resolved due to a poor-quality glass of the frozen solvent, thereby preventing the determination of the complete anisotropic spin Hamiltonian parameters for this radical anion.

Having determined the reactivity of the FLP to the individual substrates, the EPR spectrum of a full reaction mixture containing equimolar amounts of  $Mes_3P$ ,  $B(C_6F_5)_3$ , ester, and phenylacetylene was recorded (Figure 1Da). As can easily be seen, evidence of the  $[B(C_6F_5)_3]^{•-}$  radical anion is clearly observed, but there are no signals attributed to monomer or dimer phosphorus radicals present. However, it is noticed that there is additional intensity superimposed in the center of this signal ( $g_{iso} \approx 2.001$ ) which must originate from a second paramagnetic species not previously observed. Upon storage of this sample at 77 K for 30 min, the signal intensity originating from the  $[B(C_6F_5)_3]^{•-}$  radical anion was lost completely, leaving only a narrow resonance (Figure 1Db). Unfortunately, the short lifetime of this radical in solution prevented full resolution of the hyperfine coupling, but the narrow spectral width arising from only small hyperfine couplings is an indication of a carbon-based radical rather than a boron or phosphorus species (upon consideration of the theoretical isotropic hyperfine  $a_0$  values  $a_0^{(10B)} = 30.43$  mT,  $a_0^{(11B)} = 90.88$  mT, and  $a_0^{(31P)} = 474.79$  mT). The experimental spectrum is reproduced again in the SI (Figure S177) alongside simulations of the styrene and phenylacetylene radicals, using previously reported literature values.<sup>29</sup> Gratifyingly, there is reasonable agreement between the

experimental and simulated data, thereby this signal is tentatively attributed to a carbon-based radical, perhaps indicating that the reaction could be occurring through a radical mechanism.

**DFT and Kinetic Studies.** To examine the contrasting reaction pathways and to explain the experimental and EPR observations, we undertook a thorough DFT investigation of all potential reaction pathways. Calculations were performed at the SMD/B3LYP-D3/def2-TZVP//SMD/B3LYP-D3/6-31G(d) level of theory in THF and toluene solvent to examine the origin of the products. As previously reported by Slootweg et al., we found that the formation of the frustrated radical ion pair from the FLP is energetically unfavorable by 35.7 kcal/mol. This corroborates the observation that we and others<sup>6</sup> fail to see any EPR signal in solutions of  $B(C_6F_5)_3$  and  $Mes_3P$ . Very recently, Slootweg et al.<sup>5a</sup> showed that the coordination of  $B(C_6F_5)_3$  to the diaryl ester increases the electron affinity of the substrate, and the energy required for SET from  $Mes_3P$  to the methylene carbon atom is 40.0 kcal/mol.<sup>5a</sup> This is still quite large, and our calculations have revealed that, regardless of whether a diamagnetic or paramagnetic reaction pathway is ultimately operative, the first step in the reaction is the same:  $B(C_6F_5)_3$  activation of the ester to generate diaryl methylene cation **I3** (Scheme 8) and the borate anion  $[R^1CO_2B(C_6F_5)_3]^-$  with an activation energy of 10.7 kcal/mol. (See SI Figure S178 for the free-energy profile.) The energies of **I3** can be noticeably varied by changing the substitution at the para position of the aryl esters. Electron-withdrawing (*p*-CF<sub>3</sub>, **1j**), electron-withdrawing/ $\pi$ -releasing (*p*-F, **1a**), and electron-releasing (*p*-OMe, **1d**) showed different energies for **I3** (SI Figure S179–180). As expected, **I3**<sub>1d</sub> (−9.4 kcal/mol) is energetically more favorable than **I3**<sub>1j</sub> (13.5 kcal/mol) due to the electron-releasing substituents (*p*-OMe). Strongly electron-withdrawing substituents (*p*-CF<sub>3</sub>) conversely make **I3** formation thermodynamically less favorable. **I3** is then the branching point for the single- and two-electron pathways (Figure 2). The combination of diaryl methylene cation **I3** with  $Mes_3P$  can lead to three possible species in solution (Scheme 8): (i) the frustrated Lewis pair (uncoordinated **I3** +  $Mes_3P$ ), (ii) the Lewis acid–base adduct (**I4**), and (iii) the frustrated radical pair (FRP, **I5**). The energy difference and reaction barriers between these species are very low; therefore, it is likely that all three scenarios exist in equilibrium under the reaction conditions. This supports the EPR data which shows the formation of  $[Mes_3P]^{•+}$  and the  $[(P(Mes_{n=2,3})_2)]^{•+}$  dimer in the reaction of the ester with the  $Mes_3P/B(C_6F_5)_3$  FLP.

Although the carbon-based radical could not be observed in this case, we have observed a weak carbon-based radical EPR signal when reacting other esters with the  $Mes_3P/B(C_6F_5)_3$  FLP in the absence of irradiation or heat.<sup>6</sup> We then investigated the addition of the cation (**I3**) or radical (**I6**) to the alkyne. Although both pathways are feasible under the reaction conditions, the cationic pathway was lower in activation energy than the radical pathway by about 26.3–18.6 = 7.7 kcal/mol. In the case of the diamagnetic pathway, the addition of the **I3** cation to the alkyne generates **I8** via TS5. The resulting cation in **I8** is highly reactive and is rapidly trapped by the Lewis base  $Mes_3P$  generating **I9**. Finally, anti-elimination of  $[Mes_3PH]^+$  generates the cross-coupled compound and phosphonium borate salt as the final products.

The Lewis base employed is very important for the reaction to occur as seen in the screening studies. First, the ability to

form an FLP (or weak adduct) with both the Lewis acid borane and the (di)aryl methylene cation (**I3**) is critical, as other strong, less hindered Lewis acids such as  $\text{BF}_3$  do not work in the reaction. Likewise, smaller phosphines or amines tend to coordinate more strongly to the carbocation (**I3**). In addition to being able to form an FLP, the base also functions to trap reactive **I8**. Indeed, one could possibly conceive that the reaction could proceed with the Lewis acid only, whereby  $\text{R}^1\text{CO}_2^-$  accepts the proton in the last step (**I8**  $\rightarrow$  **I10**  $\rightarrow$  product, Figure 2). However, DFT calculations showed that this pathway was less favorable thermodynamically, and experimentally this reaction showed only a 22% yield with many side products formed.

We were curious to know whether both the paramagnetic and diamagnetic pathways are operative in parallel or if a diamagnetic mechanism is purely responsible for the product formation for all alkynes and the radicals observed from EPR studies were simply off-pathway intermediates. To establish this, we undertook further DFT calculations to investigate the effect of electron-withdrawing, electron-donating, and electron-neutral substituents on the ester (**1**) and the alkyne on the activation barrier for the reaction.

The energy barriers  $\text{TS4}_{\text{radical pathway}}$  and  $\text{TSS}_{\text{cationic pathway}}$  were calculated (Table 4, see SI Figure S181). Initially we varied the electronic properties of the alkyne using  $p\text{-XC}_6\text{H}_4\text{C}\equiv\text{CH}$  ( $\text{X} = \text{NO}_2, \text{CF}_3, \text{H}, \text{OMe}, \text{NMe}_2$ ) with ester **1a**. As evidence from the DFT calculations, changing the substitution at the *para* position of the arylacetylene did not make significant difference for  $\text{TS4}_{\text{radical pathway}}$  in their respective energy barrier (23.9–27.0 kcal/mol) (Table 4, entries 1–5). However, the energy barrier for  $\text{TSS}_{\text{cationic pathway}}$  changed dramatically (8.2–23.2 kcal/mol). When electron-withdrawing groups ( $p\text{-NO}_2$  and  $p\text{-CF}_3$ ) on the arylacetylene were employed, the differences between  $\text{TS4}_{\text{radical pathway}}$  and  $\text{TSS}_{\text{cationic pathway}}$  are 0.7 and 6.1 kcal/mol (Table 4, entries 1 and 2). Electronically neutral phenylacetylene exhibits a  $\text{TS4}_{\text{radical pathway}} \rightarrow \text{TSS}_{\text{cationic pathway}}$  difference of 7.7 kcal/mol (Table 3, entry 3). Electron-donating groups such as methoxy ( $\text{TS4}_{\text{radical pathway}} - \text{TSS}_{\text{cationic pathway}} = 12.1$  kcal/mol) and *N,N*-dimethylamine ( $\text{TS4}_{\text{radical pathway}} - \text{TSS}_{\text{cationic pathway}} = 18.8$  kcal/mol), on the other hand, showed a significant energy difference (Table 4, entries 4 and 5). These observations can be seen in Figure 3, which shows that for **TS4** there is a negligible change in the energy barrier when changing the electronic properties of the acetylenic substrate. This is in agreement with little charge formation on the reaction center in the radical mechanism. Conversely, for **TSS**, there is a strong positive correlation between the **TSS** energy barrier and the substituent  $\sigma_p$  constant. This is expected for the cationic pathway because a developing positive charge adjacent to the substituted phenyl ring will be stabilized by electron-donating groups (e.g.,  $p\text{-NMe}_2$  or  $p\text{-OMe}$ ) on the acetylene. As can be seen in Figure 3, **TSS** is lower than **TS4** for all substituents explored, although the difference becomes small for strongly electron-withdrawing groups.

We subsequently computed the energy barrier for the two transition states by varying the electronic properties of the aryl ester using electron-donating ( $p\text{-OMe}$ , **1d**) and electron-withdrawing ( $p\text{-CF}_3$ , **1j**) esters with electron-deficient (1-ethynyl-4-(trifluoromethyl)benzene) and electron-rich (1-ethynyl-4-methoxybenzene) acetylenes (Table 4, entries 6–9). For both esters, a smaller change in the  $\text{TS4}_{\text{radical pathway}}$  energy barrier was observed (range 22.2–27.8 kcal/mol)

compared to the  $\text{TSS}_{\text{cationic pathway}}$  energy barrier (range 8.1–25.5 kcal/mol) when changing the substituent on the phenylacetylene (Table 4, entries 6–9). As with ester **1a**, both esters disclosed a larger energy difference between the two pathways when reacted with acetylenic compounds bearing an electron-donating group ( $p\text{-OMe}$ ). Likewise, a much smaller energy difference was noted for both esters when reacted with acetylenic compounds bearing an electron-withdrawing group ( $p\text{-CF}_3$ ). Interestingly, DFT studies showed that for the case of the reaction of ester **1j** with 1-ethynyl-4-(trifluoromethyl), the radical pathway is slightly energetically more favorable compared with the cationic pathway (Table 4, entry 8). These results suggest that for electron-withdrawing arylacetylenes both paramagnetic and diamagnetic mechanisms are potentially possible, whereas for electron-rich arylacetylenes a purely diamagnetic pathway is operative.

The key difference in the two mechanisms involves the reaction of either a cationic intermediate or a radical intermediate with the arylacetylene, generating a new cationic or radical species. Whether this new intermediate is a cationic or a neutral radical species can be probed using a Hammett plot (cf. computational studies) based on substituted arylacetylenes. To gain this insight into the reaction pathway and substituent effects also from experimental evidence, we examined competition reactions among the FLP, aryl ester **1a**, and arylacetylenes  $p\text{-XC}_6\text{H}_4\text{C}\equiv\text{CH}$  bearing electron-withdrawing, electron-neutral, and electron-releasing groups. The Hammett plot requires relative rate constants for the reaction of different substituted alkynes that were obtained using a series of competition experiments. Initial competition experiments in the presence of 1.5 equiv of five arylacetylenes  $p\text{-XC}_6\text{H}_4\text{C}\equiv\text{CH}$  ( $\text{X} = \text{CF}_3, \text{F}, \text{Cl}, \text{H},$  and  $\text{OMe}$ ) were unsuccessful. The excess arylacetylene present in the reaction mixture destroyed the efficacy of the FLP system, producing a complicated reaction mixture which was not suitable for *in situ* NMR analysis. We therefore carried out three binary competition experiments with two alkynes being present at 1.5 equiv each (Table 5).

Using the optimized reaction conditions, three parallel reactions were carried out in which equimolar mixtures of (a) 1-ethynyl-4-methoxybenzene and phenylacetylene, (b) 1-ethynyl-4-(trifluoromethyl)benzene and phenylacetylene, and (c) 1-ethynyl-4-methoxybenzene and 1-ethynyl-4-(trifluoromethyl)benzene were reacted with 1 equiv of ester **1a**. The ratios of  $\text{C}_{\text{sp}^3}\text{-C}_{\text{sp}}$  cross-coupled products (**2d/2c**, **2b/2c**, and **2d/2b**) were determined from the crude reaction mixture using  $^{19}\text{F}$  NMR spectroscopy (Table 5, see SI, Figure S175). For entries 1 and 2 in Table 5, the relative integrals for the products were used to calculate the remaining equivalents for the alkynes after reaction. Using the approach developed by Ingold and Shaw<sup>30</sup> and proposed for one-pot Hammett plots by Harper and co-workers,<sup>31</sup> we obtained relative rate constants  $k_x/k_y$  for the reaction of differently substituted arylacetylenes with reaction intermediate **I3** or its equilibrium species. Entry 3 confirms that in the competition between **1a** and 1-ethynyl-4-(trifluoromethyl)benzene/1-ethynyl-4-methoxybenzene, product **2b** is undetectable, in agreement with the >200-fold difference in rate constants deduced from entries 1 and 2. The relative rate constants in Table 5 are normalized with respect to the unsubstituted alkyne and can therefore be used directly to construct a Hammett plot (using Hammett substituent constants from ref 32). The Hammett plot (Figure 4) shows a clearly negative slope of  $-6.6 \pm 1.7$ ,

suggesting the formation of a positive charge on the new intermediate, which is indicative of the cationic reaction mechanism being operative. The Hammett plot is also in agreement with the Hammett-style plot constructed using the computational data (Figure 3) for the cationic mechanism. The slope of the Hammett-style plot for TSS (Figure 3) is  $8.9 \pm 1.2 \text{ kcal mol}^{-1}$ . At  $70 \text{ }^\circ\text{C}$ , this corresponds to a Hammett  $\rho$  value of  $5.7 \pm 0.8$ . The computational data is thus in excellent agreement with the experimental findings.

Finally, we turned our attention to explaining the regioselectivity with compound **4a**. The DFT-computed (SMD/B3LYP-D3/def2-TZVP//SMD/B3LYP-D3/6-31G(d)) reaction pathways for the reaction of **I3** with 1-ethynyl-4-vinylbenzene (**4a**) and  $\text{Mes}_3\text{P}$  in THF reveal that the cationic pathway is energetically more favorable (Figure 5). After the generation of **I3**, reaction at either the alkyne or alkene site affords the corresponding  $\text{C}_{\text{sp}^3}\text{-C}_{\text{sp}}$  or  $\text{C}_{\text{sp}^3}\text{-C}_{\text{sp}^2}$  cross-coupled product. Although the transition-state energies for the **I3**-alkyne adduct (14.4 kcal/mol) and **I3**-alkene adduct (14.3 kcal/mol) are very similar, the  $\text{C}_{\text{sp}^3}\text{-C}_{\text{sp}}$  cross-coupled products are thermodynamically more stable ( $-1.4 \text{ kcal/mol}$ ) than the  $\text{C}_{\text{sp}^3}\text{-C}_{\text{sp}^2}$  cross-coupled product (5.7 kcal/mol), explaining why only the  $\text{C}_{\text{sp}^3}\text{-C}_{\text{sp}}$  cross-coupled product is observed for 1-ethynyl-4-vinylbenzene (**4a**) (Figure 5). To confirm this, we also executed single-point benchmark calculations for this transition state with a different method and solvent system (SI, Table S2), which showed results similar to those indicated in Figure 5.

The alternating site selectivity when using 1-ethynyl-2-vinylbenzene (**4d**) in differing solvents can also be highlighted in DFT studies. For the calculations, the mechanism was studied by utilizing two different solvents (toluene and THF). Experimentally, both toluene and TFT solvents lead to preferential  $\text{C}_{\text{sp}^3}\text{-C}_{\text{sp}}$  coupling. DFT calculations for the reaction of **I3** with **4d** showed that the transition-state energy for the addition of the diaryl methylene cation to the alkene or alkyne varies depending upon the solvent (Figure 6). In toluene solvent, the energy barrier for the addition of **I3** to the more nucleophilic alkyne was 3.7 kcal/mol lower in energy than the transition state for addition to the alkene (11.7 versus 15.4 kcal/mol). The converse was true for reactions in THF, whereby the addition of **I3** to the alkene was 0.5 kcal/mol lower in energy than the energy barrier for addition to the alkyne (14.7 versus 15.2 kcal/mol). We attribute this to the higher dipole moment of the calculated transition-state structure of **TS3a**, which can be stabilized better by the THF molecule. These results also explain why, in THF, the reactions were less selective, leading to a mixture of  $\text{C}_{\text{sp}^3}\text{-C}_{\text{sp}}$  and  $\text{C}_{\text{sp}^3}\text{-C}_{\text{sp}^2}$  products due to the small energy difference between the two pathways. The reactions in a solvent such as toluene (or TFT) are more selective toward  $\text{C}_{\text{sp}^3}\text{-C}_{\text{sp}}$  coupling due to the larger energy difference between the two pathways.

## CONCLUSIONS

We have demonstrated new reactivities of FLPs in the functionalization of terminal alkynes through  $\text{C}_{\text{sp}^3}\text{-C}_{\text{sp}}$  coupling reactions with aryl esters. DFT studies found that a diamagnetic pathway was most likely, although a low-energy single-electron pathway could operate to some extent. In particular, DFT studies indicate that the combination of the  $\text{Mes}_3\text{P}$ /diaryl methylene cation led to three species of similar energy in solution: the FLP (**I3**), the Lewis acid–base adduct (**I4**), and the frustrated radical pair (**I5**). According to the

Curtin–Hammett principle, the reaction proceeds predominantly via TSS from rapidly equilibrating **I3**, **I4**, **I5**, and **I6**. These rapidly equilibrating species in solution are supported by the observation of radical species of varying stabilities and lifetimes in the reaction mixture. Thus, radical species are formed in the reaction but are not making a substantial contribution on the reaction pathway to the product, with the possible exception of arylacetylenes with strongly electron-withdrawing (e.g., *p*-NO<sub>2</sub>, *p*-CF<sub>3</sub>) substituents. These observations will be of importance when designing future reactions that can switch between one- and two-electron pathways depending upon the substrate. Moreover, we observed high site selectivity when ethynyl vinylbenzene substrates were employed in these reactions. 1-Ethynyl-4-vinylbenzene substrates reacted only at the alkyne site, but 1-ethynyl-2-vinylbenzene substrates showed high selectivities depending upon the polarity of the solvent. For 1-ethynyl-2-vinylbenzene in THF,  $\text{C}_{\text{sp}^3}\text{-C}_{\text{sp}}$  coupling was observed, resulting in alkene functionalization, whereas in toluene or TFT exclusive  $\text{C}_{\text{sp}^3}\text{-C}_{\text{sp}}$  coupling and alkyne functionalization resulted. The contrasting selectivity was explained by DFT and computed transition states in the differing solvents. FLP-mediated C–C bond-forming reactions are still relatively new, but there is no doubt that advances will continue to be made in this area. This reported methodology can be utilized to generate compounds that can be subsequently employed for the synthesis of useful novel natural products where metal-free synthesis is highly desirable for avoiding metal toxicities.<sup>15,33</sup>

## ASSOCIATED CONTENT

### Supporting Information

The Supporting Information is available free of charge at <https://pubs.acs.org/doi/10.1021/jacs.1c01622>.

Detailed experimental procedures, NMR spectra, EPR data, kinetic data, and DFT data (PDF)

## AUTHOR INFORMATION

### Corresponding Author

Rebecca L. Melen – Cardiff Catalysis Institute, School of Chemistry, Cardiff University, Cardiff CF10 3AT, Cymru/Wales, United Kingdom; [orcid.org/0000-0003-3142-2831](https://orcid.org/0000-0003-3142-2831); Email: [MelenR@cardiff.ac.uk](mailto:MelenR@cardiff.ac.uk)

### Authors

Ayan Dasgupta – Cardiff Catalysis Institute, School of Chemistry, Cardiff University, Cardiff CF10 3AT, Cymru/Wales, United Kingdom

Katarina Stefkova – Cardiff Catalysis Institute, School of Chemistry, Cardiff University, Cardiff CF10 3AT, Cymru/Wales, United Kingdom

Rasool Babaahmadi – School of Natural Sciences-Chemistry, University of Tasmania, Hobart, Tasmania 7001, Australia; [orcid.org/0000-0002-2580-6217](https://orcid.org/0000-0002-2580-6217)

Brian F. Yates – School of Natural Sciences-Chemistry, University of Tasmania, Hobart, Tasmania 7001, Australia

Niklaas J. Buurma – Cardiff Catalysis Institute, School of Chemistry, Cardiff University, Cardiff CF10 3AT, Cymru/Wales, United Kingdom

Alireza Ariaifard – School of Natural Sciences-Chemistry, University of Tasmania, Hobart, Tasmania 7001, Australia

Emma Richards – Cardiff Catalysis Institute, School of Chemistry, Cardiff University, Cardiff CF10 3AT, Cymru/Wales, United Kingdom

Wales, United Kingdom; [orcid.org/0000-0001-6691-2377](https://orcid.org/0000-0001-6691-2377)

Complete contact information is available at:  
<https://pubs.acs.org/10.1021/jacs.1c01622>

## Funding

A.D., K.S., and R.L.M. acknowledge the EPSRC for an Early Career Fellowship for funding (EP/R026912/1). A.D., E.R., and R.L.M. thank the Leverhulme Trust for a research project grant (RPG-2020-016). A.A., B.F.Y., and R.B. thank the Australian Research Council (ARC) for project funding (DP180100904) and the Australian National Computational Infrastructure and the University of Tasmania for the generous allocation of computing time. Information about the data that underpins the results presented in this article, including how to access them, can be found in the Cardiff University data catalogue. This can be found at <http://doi.org/10.17035/d.2021.0130087985>.

## Notes

The authors declare no competing financial interest.

## REFERENCES

- (1) For the first report, see (a) Welch, G. C.; Juan, R. R. S.; Masuda, J. D.; Stephan, D. W. Reversible, metal-free hydrogen activation. *Science* **2006**, *314*, 1124–1126. For reviews, see (b) Jupp, A. R.; Stephan, D. W. New directions for frustrated Lewis pair chemistry. *Trends in Chemistry* **2019**, *1*, 35–48. (c) Scott, D. J.; Fuchter, M. J.; Ashley, A. E. Designing effective ‘frustrated Lewis pair’ hydrogenation catalysts. *Chem. Soc. Rev.* **2017**, *46*, 5689–5700. (d) Stephan, D. W. The broadening reach of frustrated Lewis pair chemistry. *Science* **2016**, *354*, aaf7229. (e) Stephan, D. W. Frustrated Lewis pairs. *J. Am. Chem. Soc.* **2015**, *137*, 10018–10032. (f) Stephan, D. W.; Erker, G. Frustrated Lewis pair chemistry: development and perspectives. *Angew. Chem., Int. Ed.* **2015**, *54*, 6400–6441. (g) Stephan, D. W. Frustrated Lewis pairs: from concept to catalysis. *Acc. Chem. Res.* **2015**, *48*, 306–316.
- (2) For selected reviews, see (a) Lam, J.; Szkop, K. M.; Mosaféria, E.; Stephan, D. W. FLP catalysis: main group hydrogenations of organic unsaturated substrates. *Chem. Soc. Rev.* **2019**, *48*, 3592–3612. (b) Power, P. Main-group elements as transition metals. *Nature* **2010**, *463*, 171–177. (c) Stephan, D. W.; Erker, G. Frustrated Lewis pairs: Metal-free hydrogen activation and more. *Angew. Chem., Int. Ed.* **2010**, *49*, 46–76. (d) Stephan, D. W. Frustrated Lewis pairs: a new strategy to small molecule activation and hydrogenation catalysis. *Dalton Trans* **2009**, *2009*, 3129–3136. Also see (e) Wilkins, L. C.; Melen, R. L. Small Molecule Activation with Frustrated Lewis Pairs. *Encyclopedia of Inorganic and Bioinorganic Chemistry*; John Wiley & Sons, Ltd., 2017; pp 1–24.
- (3) For selected reviews, see (a) Carden, J. L.; Dasgupta, A.; Melen, R. L. Halogenated triarylboranes: synthesis, properties and applications in catalysis. *Chem. Soc. Rev.* **2020**, *49*, 1706–1725. (b) Paradies, J. Mechanisms in frustrated Lewis pair-catalyzed reactions. *Eur. J. Org. Chem.* **2019**, *2019*, 283–294. (c) Scott, D. J.; Fuchter, M. J.; Ashley, A. E. Designing effective ‘frustrated Lewis pair’ hydrogenation catalysts. *Chem. Soc. Rev.* **2017**, *46*, 5689–5700.
- (4) For reviews, see (a) Hoshimoto, Y.; Ogoshi, S. Triarylborane-catalyzed reductive *N*-alkylation of amines: A perspective. *ACS Catal.* **2019**, *9*, 5439–5444. (b) Fyfe, J. W. B.; Watson, A. J. B. Merging new organoborane chemistry with living radical polymerization. *Chem.* **2017**, *3*, 31–55. For selected articles, see (c) Khan, I.; Manzotti, M.; Tizzard, G. J.; Coles, S. J.; Melen, R. L.; Morrill, L. C. Frustrated Lewis pair (FLP)-catalyzed hydrogenation of Aza-Morita–Baylis–Hillman adducts and sequential organo-FLP catalysis. *ACS Catal.* **2017**, *7*, 7748–7752. (d) L egar e, M.-A.; Courtemanche, M.-A.; Rochette,  . Fontaine, F.-G. Metal-free catalytic C–H bond activation and borylation of heteroarenes. *Science* **2015**, *349*, 513–516. (e) Shi, L.; Zhou, Y.-G. Enantioselective metal-free hydrogenation catalyzed by chiral frustrated Lewis pairs. *ChemCatChem* **2015**, *7*, 54–56.
- (5) (a) Holtrop, F.; Jupp, A. R.; Kooij, B. J.; van Leest, N. P.; de Bruin, B.; Slootweg, J. C. Single-electron transfer in frustrated Lewis pair chemistry. *Angew. Chem., Int. Ed.* **2020**, *59*, 22210–22216. (b) Holtrop, F.; Jupp, A. R.; van Leest, N. P.; Dominguez, M. P.; Williams, R.; Brouwer, M. A. M.; de Bruin, B.; Ehlers, A. W.; Slootweg, J. C. Photoinduced and thermal single-electron transfer to generate radicals from frustrated Lewis pairs. *Chem. - Eur. J.* **2020**, *26*, 9005–9011. (c) Liu, L. L.; Stephan, D. W. Radicals derived from Lewis acid/base pairs. *Chem. Soc. Rev.* **2019**, *48*, 3454–3463. (d) Schilter, D. Frustration leads to radical behaviour. *Nat. Rev. Chem.* **2018**, *2*, 255. (e) Hamilton, H. B.; Wass, D. F. How important are radical mechanisms in frustrated Lewis pair chemistry? *Chem.* **2017**, *3*, 198–210. (f) M enard, G.; Hatnean, J. A.; Cowley, H. J.; Lough, A. J.; Rawson, J. M.; Stephan, D. W. C–H Bond activation by radical ion pairs derived from R<sub>3</sub>P/Al(C<sub>6</sub>F<sub>5</sub>)<sub>3</sub> frustrated Lewis pairs and N<sub>2</sub>O. *J. Am. Chem. Soc.* **2013**, *135*, 6446–6449. Also see (g) Warren, T. H.; Erker, G. *Frustrated Lewis Pairs II: Expanding the Scope*; Topics in Current Chemistry 334; Springer: Berlin, 2013. (h) Piers, W. E.; Marwitz, A. J. V.; Mercier, L. G. Mechanistic Aspects of Bond Activation with Perfluoroarylboranes. *Inorg. Chem.* **2011**, *50*, 12252–12262. (i) Aramaki, Y.; Imaizumi, N.; Hotta, M.; Kumagai, J.; Ooi, T. Exploiting single-electron transfer in Lewis pairs for catalytic bond-forming reactions. *Chem. Sci.* **2020**, *11*, 4305–4311.
- (6) Soltani, Y.; Dasgupta, A.; Gazis, T. A.; Ould, D. M. C.; Richards, E.; Slater, B.; Stefkova, K.; Vladimirov, V. Y.; Wilkins, L. C.; Willcox, D.; Melen, R. L. Radical reactivity of frustrated Lewis pairs with diaryl esters. *Cell Reports Physical Science* **2020**, *1*, 100016.
- (7) (a) Fasano, V.; Curless, L. D.; Radcliffe, J. E.; Ingleson, M. J. Frustrated Lewis pair mediated 1,2-hydrocarbation of alkynes. *Angew. Chem., Int. Ed.* **2017**, *56*, 9202–9206. (b) Yanagisawa, T.; Mizuhata, Y.; Tokitoh, N. Additive-free conversion of internal alkynes by phosphanylaluminanes: Production of phosphorus/Aluminum frustrated Lewis pairs. *ChemPlusChem* **2020**, *85*, 933–942. (c) Jiang, C.; Blacque, O.; Berke, H. Activation of terminal alkynes by frustrated Lewis pairs. *Organometallics* **2010**, *29*, 125–133. (d) Dureen, M. A.; Stephan, D. W. Terminal alkyne activation by frustrated and classical Lewis acid/phosphine pairs. *J. Am. Chem. Soc.* **2009**, *131*, 8396–8397.
- (8) Chernichenko, K.; Madar asz, A.; P apai, I.; Nieger, M.; Leskela, M.; Repo, T. A frustrated-Lewis-pair approach to catalytic reduction of alkynes to *cis*-alkenes. *Nat. Chem.* **2013**, *5*, 718–723.
- (9) For examples, see (a) Beattie, J. W.; Wang, C.; Zhang, H.; Krogman, J. P.; Foxman, B. M.; Thomas, C. M. Dimerization of terminal alkynes promoted by a heterobimetallic Zr/Co complex. *Dalton Trans* **2020**, *2020*, 2407–2411. (b) Sivaguru, P.; Cao, S.; Babu, K. R.; Bi, X. Silver-catalyzed activation of terminal alkynes for synthesizing nitrogen-containing molecules. *Acc. Chem. Res.* **2020**, *53*, 662–675. (c) Ansell, M. B.; Navarro, O.; Spencer, J. Transition metal catalyzed element–element additions to alkynes. *Coord. Chem. Rev.* **2017**, *336*, 54–77. (d) Trost, B. M.; Masters, J. T. Transition metal-catalyzed couplings of alkynes to 1,3-enynes: modern methods and synthetic applications. *Chem. Soc. Rev.* **2016**, *45*, 2212–2238. (e) Halliday, C. J. V.; Lynam, J. M. Gold–alkynyls in catalysis: alkyne activation, gold cumulenes and nuclearity. *Dalton Trans* **2016**, *2016*, 12611–12626.
- (10) For reviews, see (a) Chinchilla, R.; N ajera, C. The Sonogashira reaction: A booming methodology in synthetic organic chemistry. *Chem. Rev.* **2007**, *107*, 874–922. (b) Chinchilla, R.; N ajera, C. Recent advances in Sonogashira reactions. *Chem. Soc. Rev.* **2011**, *40*, 5084–5121. For selected articles, see (c) Zhang, Z.-H.; Dong, X.-Y.; Du, X.-Y.; Gu, Q.-S.; Li, Z.-L.; Liu, X.-Y. Copper-catalyzed enantioselective Sonogashira-type oxidative cross-coupling of unactivated C(sp<sup>3</sup>)-H bonds with alkynes. *Nat. Commun.* **2019**, *10*, 5689. (d) Correia, C. A.; Li, C.-J. Copper-catalyzed cross-dehydrogenative coupling (CDC) of alkynes and benzylic C–H Bonds. *Adv. Synth. Catal.* **2010**, *352*, 1446–1450.

- (11) (a) Gazvoda, M.; Virant, M.; Pinter, B.; Košmrlj, J. Mechanism of copper-free Sonogashira reaction operates through palladium-palladium transmetalation. *Nat. Commun.* **2018**, *9*, 4814. (b) Huang, H.; Liu, H.; Jiang, H.; Chen, K. Rapid and efficient Pd-catalyzed Sonogashira coupling of aryl chlorides. *J. Org. Chem.* **2008**, *73*, 6037–6040.
- (12) (a) Sawama, Y.; Goto, R.; Nagata, S.; Shishido, Y.; Monguchi, Y.; Sajiki, H. Chemoselective and direct functionalization of methyl benzyl ethers and unsymmetrical dibenzyl ethers by using iron trichloride. *Chem. - Eur. J.* **2014**, *20*, 2631–2636. (b) Xiang, S.-K.; Zhanga, L.-H.; Jiao, N.  $sp-sp^3$  C–C bond formation via  $Fe(OTf)_3/TfOH$  cocatalyzed coupling reaction of terminal alkynes with benzylic alcohols. *Chem. Commun.* **2009**, 2009, 6487–6489.
- (13) For a selected review, see (a) Thomas, A. M.; Sujatha, A.; Anilkumar, G. Recent advances and perspectives in copper-catalyzed Sonogashira coupling reactions. *RSC Adv.* **2014**, *4*, 21688–21698. For a selected article, see (b) Cao, Y.-X.; Dong, X.-Y.; Yang, J.; Jiang, S.-P.; Zhou, S.; Li, Z.-L.; Chen, G.-Q. A Copper-catalyzed Sonogashira coupling reaction of diverse activated alkyl halides with terminal alkynes under ambient conditions. *Adv. Synth. Catal.* **2020**, *362*, 2280–2284.
- (14) Nan, G.; Zhou, J. Indium(III) catalyzed direct  $sp^3-sp$  C–C bond formation from alcohols and terminal alkynes. *Lett. Org. Chem.* **2013**, *10*, 555–561.
- (15) Fisher, K. M.; Bolshan, Y. Brønsted acid-catalyzed reactions of trifluoroborate salts with benzhydryl alcohols. *J. Org. Chem.* **2015**, *80*, 12676–12685.
- (16) Kabalka, G. W.; Yao, M.-L.; Borella, S. Substitution of hydroxyl groups with alkynyl moieties using alkynylboron dihalides: An efficient approach to secondary alkylacetylene derivatives. *Org. Lett.* **2006**, *8*, 879–881.
- (17) Malkoch, M.; Thibault, R. J.; Drockenmuller, E.; Messerschmidt, M.; Voit, B.; Russell, T. P.; Hawker, C. J. Orthogonal approaches to the simultaneous and cascade functionalization of macromolecules using click chemistry. *J. Am. Chem. Soc.* **2005**, *127*, 14942–14949.
- (18) Barluenga, J.; Andina, F.; Aznar, F.; Valdés, C. New cascade processes on group 6 Fischer-type carbene complexes: Cyclopropanation and metathesis reactions. *Org. Lett.* **2007**, *9*, 4134–4146.
- (19) Dasgupta, A.; Stefkova, K.; Babaahmadi, R.; Gierlich, L.; Ariafard, A.; Melen, R. L. Triarylborane catalyzed alkenylation reaction of aryl esters with diazo-compounds. *Angew. Chem., Int. Ed.* **2020**, *59*, 15492–15496.
- (20) Follet, E.; Mayer, P.; Stephenson, D. S.; Ofial, A. R.; Berionni, G. Reactivity-tuning in frustrated Lewis pairs: Nucleophilicity and Lewis basicity of sterically hindered phosphines. *Chem. - Eur. J.* **2017**, *23*, 7422–7427.
- (21) Liu, L.; Cao, L. L.; Shao, Y.; Menard, G.; Stephan, D. W. A radical mechanism for frustrated Lewis pair reactivity. *Chem.* **2017**, *3*, 259–267.
- (22) Pan, X.; Chen, X.; Li, T.; Li, Y.; Wang, X. Isolation and X-ray crystal structures of triarylphosphine radical cations. *J. Am. Chem. Soc.* **2013**, *135*, 3414–3417.
- (23) Lyons, A. R.; Symons, M. C. R. Unstable intermediates. Part 117 – Electron spin resonance studies of dimeric ( $\sigma^*$ ) radicals of type  $R_3X-XR_3$  with a three electron X–X bond, when X is phosphorus or arsenic. *J. Chem. Soc., Faraday Trans. 2* **1972**, *68*, 1589–1594.
- (24) Gara, W. B.; Roberts, B. R. An electron spin resonance study of the electrochemical oxidation of phosphorus(III) compounds. *J. Chem. Soc., Perkin Trans. 2* **1978**, 1978, 150–154.
- (25) Symons, M. C. R.; Tordo, P.; Wyatt, J. The structure of diphosphine radical cations. *J. Organomet. Chem.* **1993**, *443*, C29–C32.
- (26) Culcasi, M.; Gronchi, G.; Tordo, P. Tetraaryldiphosphine cation radicals. electrochemical generation and ESR study. *J. Am. Chem. Soc.* **1985**, *107*, 7191–7193.
- (27) (a) Sipe, H. J., Jr.; Hwang, J. S.; Tsonls, C. P.; Klsper, L. D. Electron paramagnetic resonance studies of thermally produced radicals in phenylacetylene. *J. Phys. Chem.* **1982**, *86*, 4017–4019.
- (b) Buick, A. R.; Kemp, T. J.; Stone, T. J. Electron spin resonance spectra of radical anions of styrene and related compounds. *J. Phys. Chem.* **1970**, *74*, 3439–3444.
- (28) Kwaan, R. J.; Harlan, C. J.; Norton, J. R. Generation and characterization of the tris(pentafluorophenyl)borane radical anion. *Organometallics* **2001**, *20*, 3818–3820.
- (29) For the styryl radical, see (a) Bennett, J. E.; Howard, J. A. ESR spectrum of the  $\alpha$ -styryl radical. *Chem. Phys. Lett.* **1971**, *9*, 460–462. For the phenylacetylene radical, see (b) Sipe, H. J.; Kispert, L. D.; Hwang, J. S.; Tsonis, C. P. Electron Paramagnetic Resonance studies of thermally produced radicals in phenylacetylene. *J. Phys. Chem.* **1982**, *86*, 4017–4019.
- (30) Ingold, C. K.; Shaw, F. R. CCCLXXXVIII.—The nature of the alternating effect in carbon chains. Part XXII. An attempt further to define the probable mechanism of orientation in aromatic substitution. *J. Chem. Soc.* **1927**, 0, 2918–2926.
- (31) Yau, H. M.; Croft, A. K.; Harper, J. B. One-pot' Hammett plots: a general method for the rapid acquisition of relative rate data. *Chem. Commun.* **2012**, 48, 8937–8939.
- (32) Hansch, C.; Leo, A.; Taft, R. W. A survey of Hammett substituent constants and resonance and field parameters. *Chem. Rev.* **1991**, *91*, 165–195.
- (33) (a) Miao, M.; Jin, M.; Chen, P.; Wang, L.; Zhang, S.; Ren, H. Iron(III)-Mediated Bicyclization of 1,2-Allenyl Aryl Ketones: Assembly of Indanone-Fused Polycyclic Scaffolds and Dibenzo[a,e]-pentalene Derivatives. *Org. Lett.* **2019**, *21*, 5957–5961. (b) Martins, G. M.; Back, D. F.; Kaufman, T. S.; Silveira, C. C.  $SeCl_2$ -Mediated Approach Toward Indole-Containing Polysubstituted Selenophenes. *J. Org. Chem.* **2018**, *83*, 3252–3264.